Characterization of oxide-supported Cu by infrared measurements on adsorbed CO

Niels D. Nielsen[a], Thomas E.L. Smitshuysen[b], Christian D. Damsgaard[b,c], Anker D. Jensen[a], Jakob M. Christensen[a,*]

[a] *Department of Chemical and Biochemical Engineering, Technical University of Denmark, Søltofts Plads Building 229, 2800 Kgs. Lyngby, Denmark*
[b] *Department of Physics, Technical University of Denmark, Fysikvej Building 311, 2800 Kgs. Lyngby, Denmark*
[c] *National Centre for Nano Fabrication and Characterization, Technical University of Denmark, Fysikvej Building 307, 2800 Kgs. Lyngby, Denmark*

ARTICLE INFO

ABSTRACT

Infrared spectroscopy on CO chemisorbed on Raney Cu and materials with Cu dispersed as nanoparticles on oxide supports was used to evaluate support effects on the Cu surface properties. The C-O frequency (ν_{C-O}) is sensitive to the charge on the adsorption site with ν_{C-O} being high on Cu^+, intermediate on Cu^0, and low on Cu^-, whereby this method can probe the charging state of the Cu surface. The Raney Cu reference demonstrates the complex analysis of the IR band intensity, which can be susceptible to dipole coupling. This means that the most intense IR bands may be higher frequency bands strengthened by such coupling effects rather than the bands arising from the most abundant sites. The ν_{C-O} of the major band attributable to CO adsorbed on the metallic surface follows the order: Cu/SiO_2 > Raney Cu > Cu/Al_2O_3 > Cu/TiO_2. Given the charge-frequency relationship these support-dependent frequency shifts are attributed to changes in the charging of the Cu surface caused by support effects. The Cu surface is more electron deficient for Cu/SiO_2 and electron enriched for Cu/TiO_2. For the $Cu/ZnO(/Al_2O_3)$ samples, which are important as industrial methanol synthesis catalysts, band assignments are complicated by a low ν_{C-O} on Cu^+ sites connected to the ZnO matrix. However, $Cu/ZnO(/Al_2O_3)$ has a spectral feature at 2065-68 cm^{-1}, which is a lower frequency than observed in the Cu single crystal studies in the literature and thus indicative of a negative charging of the Cu surface in such systems. Experiments with co-adsorption of CO and electron-withdrawing formate on Cu/ZnO and Cu/SiO_2 show that ν_{C-O} in the adsorbed CO shifts upwards with increasing HCOO coverage. This illustrates that the surface charge is donated to the electron-withdrawing formate adsorbate, and as a result co-adsorbed CO experiences a more charge depleted Cu surface that yields higher ν_{C-O}. The support-dependent surface charging may thus affect the interaction with adsorbates on the metal surface and thereby impact the catalytic properties of the Cu surface. Dilution of the samples in KBr, which has been used in many studies in the literature, had pronounced effects on the spectra. The presence of KBr leads to an increase in ν_{C-O} indicative of an electron depleted surface attributed to transfer of electron-withdrawing bromine species from KBr to the sample.

1. Introduction

Materials with copper dispersed as nanoparticles on oxide supports are of great practical importance as catalysts for reactions such as methanol synthesis and the water-gas shift reaction. In these two reactions catalytic activity only emerges once the copper is reduced to the metallic state [1,2], and catalytic activity scales linearly with the Cu surface area [3–8], which strongly indicates that the reaction occurs on the metallic surface. However, the support used to disperse the Cu has a major impact on the catalytic activity and may cause order of magnitude changes to the rate of the reaction on the Cu surface [9–13]. It is

therefore important to investigate, how the properties of the Cu surface depend on the underlying support. Infrared spectroscopy of CO adsorbed on the surface as a probe molecule is a valuable technique because of the high sensitivity of the C-O stretching frequency (ν_{C-O}) to the nature of the adsorption site. Focusing on the dominant on-top bonding of CO, the most important factor for the C-O frequency on Cu is the charge on the adsorption site. This is illustrated by Fig. 1, which shows how high C-O frequencies correspond to more positively charged adsorption sites, while progressively lower C-O frequencies are characteristic of zero-valent and negatively charged Cu sites.

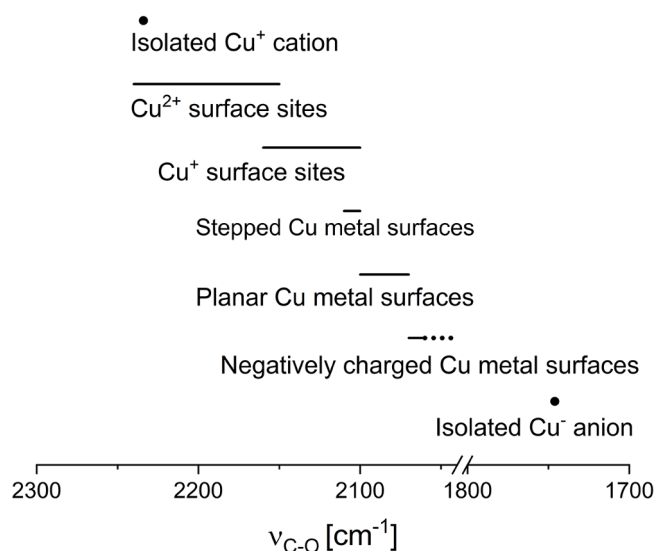The charge on the Cu site depends on the surroundings. CO

Fig. 1. C-O stretching frequencies (ν_{C-O}) for CO adsorbed on Cu surfaces or on isolated Cu ions (in frozen Ne) based on reports in the literature [14–19]. The values are for the predominant linear, on-top bonding of CO.

adsorbed on fully developed Cu^+ sites is associated with frequencies above ca. 2105-2110 cm^{-1}, but Davydov [20] observed that Cu cations linked to a basic oxide (MgO or ZnO) appeared to be $Cu^{\delta+}$ sites with a limited positive charge and gave $\nu_{C-O} < 2100$ cm^{-1} in the adsorbed CO. This can be rationalized from the Lewis definition of a base as an electron donor that thus limits the positive charge on the Cu cation. On the metallic surface the morphology is also important. According to the theory of Smoluchowski [21] the electronic cloud at the metal surface smoothens out, which means that charge flows from protrusions, such as step atoms to the lower lying facets. As a result the step atoms become positively charged $Cu^{\delta+}$ sites. This positive charge on protrusions explains, why stepped Cu single crystal surfaces exhibit the highest C-O frequencies among metallic surfaces - near the transition to fully developed Cu^+ sites (Fig. 1). The same partial charging applies for other protrusions in nanoparticles, such as edges and corners [22,23]. On the low-index, planar Cu surfaces the frequency is generally found in the 2070-2100 cm^{-1} range [16]. The highest frequencies occur on the Cu (110) surface that also has protruding rows of atoms. If the metal surface is negatively charged, the C-O stretches shift to lower frequencies. By theoretical calculations Head-Gordon and Tully [17] observed that the C-O frequency in CO adsorbed on a Cu_{14} cluster was lowered by 127 cm^{-1}, when the cluster was negatively charged corresponding to an electric field of -0.5 V/Å.

The relationship between surface charging state and frequency can be rationalized through the Blyholder model [24]. The metal-CO bond is dominated by donation from the 5σ orbital of CO to the metal surface and back donation from the metal surface to the 2π* orbitals of CO. Both the 5σ and 2π* orbitals are anti-bonding with respect to the internal C-O bond [25]. Hence, more positively charged sites will receive more donation from the 5σ orbital and back donate less to the 2π* orbitals, which results in strengthening of the C-O bond and a higher stretching frequency (due to greater removal from a CO anti-bonding orbital). More negatively charged sites will oppositely receive less 5σ donation and back donate more leading to a lower C-O frequency (due to greater donation to a CO anti-bonding orbital).

Although providing valuable information, there are also important factors to consider in the interpretation of the IR spectra of adsorbed CO. Possibly the most important effect is dipole coupling. The vibrations of the adsorbed molecules are coupled by the electrostatic fields from their radiation induced dipoles [26]. Hollins [27] found that if the surface contains two different sites giving C-O frequencies in close proximity, the higher frequency is subjected to constructive

interference resulting in enhanced absorbance intensity, whereas the lower frequency experiences destructive interference and weakens. As an example Hollins and co-workers [26,27] showed that if the surface contains just a few percent of high C-O frequency sites, such as the $Cu^{\delta+}$ atoms at steps, the positive interference from dipole coupling causes these high C-O frequency sites to dominate the recorded IR spectrum completely. The CO on the planar facets, which has a lower C-O frequency and therefore receives destructive interference, will only be seen as a minor shoulder in the spectrum despite constituting the majority of the adsorption sites. For complex supported samples with a variety of facets the main spectral features from CO on the metallic surface must therefore be expected to represent adsorption at the higher frequency sites at surface protrusions (e.g. steps or the protruding rows in (110) facets). Experimentally it is observed [28] that the strengthening of the high frequency band induced by dipole coupling increases with adsorbate coverage as more adsorbates contribute to the interference phenomena. A second important factor to consider is the preferential bonding. In the case of copper, positively charged Cu^+ sites bind CO stronger than metallic Cu sites, which can be attributed to the greater donation from the 5σ orbital of CO to the Cu^+ site [29]. It must therefore be expected that the positively charged Cu sites are occupied first upon exposure to CO and are the last to be vacated upon desorption.

There have been previous comparative studies [30,31] of support effects on Cu, but these studies have proposed explanations that varied from adsorption dominantly on the metallic surface to full oxide decoration of the Cu particles, and the available studies thus offer no unified conclusions. Consequently it is still highly necessary to examine the issue of support effects in Cu-based materials. Additionally, a significant part of the published literature using infrared spectroscopy has used samples diluted in KBr. However, the presence of KBr has been reported [32,33] to induce significant chemical modifications to the investigated sample and its properties. It is therefore also relevant to assess the effect of KBr to evaluate the validity of the results in the literature.

Here we conduct FTIR investigations of CO adsorbed on Cu dispersed on a variety of supports (SiO_2, Al_2O_3, ZnO(/Al_2O_3) and TiO_2) using high surface area samples representative of catalytic materials. The main aim is to identify the primary IR band from CO adsorbed on the metallic Cu surface of each sample and to detect the presence of any support effects. Low temperature measurements are used to obtain spectra of CO on Raney Cu to assess the intrinsic properties of Cu for comparison to the supported samples. Experiments with co-adsorption of formate and CO were used to gain further insight into the Cu surface properties. Furthermore, experiments with controlled addition of KBr were conducted to evaluate the effect of dilution by KBr used in much of the previous IR work in the literature.

2. Materials and methods

2.1. Materials

Flows are reported with reference to normal (N) conditions equal to 273.15 K and 1 atm. of pressure. All supported Cu samples were prepared from the nitrate ($Cu(NO_3)_2 \cdot 3H_2O \geq 98.6\%$ from Alfa Aesar). Cu/ZnO, Cu/ZnO/Al_2O_3 and Cu/Al_2O_3 samples were synthesized by co-precipitation methods with metal nitrate precursors (using Zn$(NO_3)_2 \cdot 6H_2O \geq 98\%$, Al$(NO_3)_3 \cdot 9H_2O \geq 98\%$ from Sigma Aldrich) and a precipitating agent (Na_2CO_3, $\geq$ 99.8% from Sigma Aldrich). Precipitation conditions were adapted from the optimal conditions reported by Baltes and co-workers [4]. The precipitation was conducted by dripping nitrate solution and precipitation agent into a stirred beaker initially containing 500 mL of demineralized water as a temperature buffer. The precipitation was conducted at pH = 6.5 and T = 338 K until the nitrate solution was consumed and the precipitate was then aged at this temperature for 1 hour with unrestricted pH. Cu/

TiO$_2$ was prepared by deposition-precipitation using similar synthesis parameters, but with TiO$_2$ anatase powder (nanopowder, 21 nm particle size from Sigma Aldrich) added to the initial 500 mL of water. The aged precipitates for Cu/ZnO (10 wt% Cu), Cu/ZnO/Al$_2$O$_3$ (63.0 wt% Cu, 32.5 wt% Zn, 4.5 wt% Al), Cu/Al$_2$O$_3$ (20 wt% Cu), and Cu/TiO$_2$ (20 wt% Cu) were filtered and thoroughly washed using demineralized water followed by overnight drying at 313 K before calcination. Dried samples were loaded into alumina crucibles and calcined in a tubular furnace using an air flow of 1 NL/min, while ramping the temperature by 2 K/min (1 K/min for Cu/Al$_2$O$_3$) to the calcination temperature of 573 K (603 K for Cu/Al$_2$O$_3$) which was held for three hours before cooling. After calcination the samples were pressed, crushed and sieved to 150-300 μm. Cu/SiO$_2$ (10 wt% Cu) was prepared by impregnation using crushed and sieved (150-300 μm) SiO$_2$ carrier particles (SS61138, 250 m^2/g, from Saint Gobain) with the Cu nitrate precursor before drying overnight at 313 K and calcination by the same procedure as for the other samples.

Raney Cu (98.9 wt% Cu, 0.81 wt% Al, 0.1 wt% Fe, 0.05 wt% Ni) was purchased as an aqueous solution from Strem Chemicals and was pre-dried in air at room temperature in a fume hood to obtain a dry state before loading. Further characterization of this sample is reported elsewhere [34].

FTIR grade KBr was purchased from Sigma Aldrich and sieve fractionated to 150-300 μm before use.

2.2. Methods

Generally the samples were pre-reduced/activated in situ by hydrogen at atmospheric pressure prior to measurements on reduced samples. The samples were heated (1 K/min) in 5% H$_2$/N$_2$ to first 448 K and secondly to 523 K with holding times of generally 30-180 min at both temperatures until no further water evolution could be detected. For Cu/Al$_2$O$_3$ the standard procedure was followed by a subsequent treatment in 100% H$_2$ at 523 K until no further water evolution could be detected.

The exposed Cu surface areas of the pre-reduced samples were measured by the N$_2$O Reactive Frontal Chromatography (RFC) method [35] using a Quantachrome IQ$_2$ setup. After pre-reduction the samples were subsequently cooled in He to 333 K and here exposed to a 19 Nml/min flow of 1% N$_2$O/He to determine the Cu surface area from the oxygen uptake. The Cu surface area calculations were based on the N$_2$O consumption, using a Cu:O stoichiometry of 2:1 [36] and an average Cu surface atom density of $1.47 \cdot 10^{19}$ atoms/(m^2 Cu) [37].

In situ XRD was performed using an X'Pert Pro diffractometer from Malvern Panalytical with a Cu$_{K\alpha}$ anode and an installed XRK 900 in situ cell from Anton Paar and applied to determine the Cu crystallite size based on the Scherrer method. In situ XRD also verified complete Cu reduction with the applied activation method (Fig. S1-S6). The effluent gas was analyzed by a Pfeiffer quadrupole mass spectrometer. Prior to analyses samples were activated by the same hydrogen concentrations as outlined previously by mixing 99.9999% He and 99.9999% H$_2$ from Air Liquide Denmark. The Cu crystallite size was estimated from the Scherrer equation [38] using a Scherrer constant of 0.9 [39,40] and correction for an instrumental broadening of maximally 0.1°. The Inorganic Crystal Structure Database [41] with the collection code written in parentheses is applied to identify observed XRD peaks. XRD patterns featured a growing baseline with increasing 2θ especially for the samples with high Cu weight percentage due to fluorescence from the sample matching the Cu$_{K\alpha}$ anode.

Infrared spectroscopy experiments were conducted with a domed reactor cell and Praying Mantis Diffuse Reflectance Infrared Fourier Transform Spectroscopy (DRIFTS) unit from Harrick Scientific Products using a Nicolet iS50 FTIR spectrometer with a liquid N$_2$ cooled MCT detector. Measured spectra were an average of 76 scans with a resolution of 4 cm^{-1}. In a standard experiment the Cu samples were loaded and compacted in the sample cup of the reactor cell before

experiments. Gasses ($\geq$ 99.999% He with < 2 ppm O$_2$, 9.50% CO/Ar with < 3 ppm O$_2$, H$_2$, 5.01% H$_2$/N$_2$ with < 2 ppm O$_2$, 9.00% CO$_2$/N$_2$ with < 3 ppm O$_2$, $\geq$ 99.999% H$_2$ with < 2 ppm O$_2$, $\geq$ 99.999% N$_2$ with < 2 ppm O$_2$) were obtained from Air Liquide Denmark and dosed via Brooks SLA5850 mass flow controllers. The gas passes through an active carbon filter immediately before entering the reactor cell. The effluent gas from the reactor cell was analyzed by a Hiden HPR-20 EGA mass spectrometer (MS).

All measurements were conducted at atmospheric pressure starting with the hydrogen activation procedure outlined above. For CO adsorption experiments, the activated samples were cooled in He to the CO adsorption temperature, where a background spectrum was recorded in He prior to CO exposure. The samples were then exposed to 0.4 mbar CO balanced in inert gas and analyzed as spectra (in Kubelka-Munk units) using the aforementioned background. The typical measurement temperature of 276 K was achieved from adjusting the temperature of the thermostatic bath supplying the cooling water circulating through the IR cell.

Low-temperature measurements were used for Raney Cu. These measurements were conducted using a CHC-CHA-3 reaction chamber (Harrick Scientific Products) that includes a liquid N$_2$ container connected through a cold finger to the low temperature reaction chamber. Pre-reduced Raney Cu was held in an N$_2$ atmosphere at room temperature before cooling to a temperature of 152-153 K. At this temperature a background spectrum was recorded in flowing N$_2$ before exposure to 0.4 mbar CO. Subsequently the cell was purged with N$_2$ and absorbance spectra of the adsorbed CO were recorded using the background measured at the same temperature in N$_2$ prior to CO exposure.

To aid the distinction between contributions from metallic and oxidized sites, measurements were conducted on oxidized samples (to eliminate the metallic contributions) and after a harsher reduction in CO to help eliminate oxide contributions. Two types of measurements on oxidized samples were conducted. In one type of measurement the CuO/SiO$_2$ and CuO/TiO$_2$ oxide precursors were instead of pre-reduction only outgassed in flowing He at 373 K until no further water evolution could be detected and then cooled in He to 276 K. Here adsorption of 0.4-100 mbar CO in stepwise increasing CO concentration was conducted. For the other type of measurement on oxidized samples Raney Cu, Cu/Al$_2$O$_3$, Cu/ZnO/Al$_2$O$_3$, and Cu/SiO$_2$ were activated by the normal pre-reduction and then re-oxidized at room temperature by exposure to a flow of 9% CO$_2$/N$_2$. After flushing of the cell with He at room temperature, the CO adsorption was then conducted with 0.4-100 mbar CO in stepwise increasing concentration at 276 K (152-153 K for Raney Cu).

For tests with a harsher reductive treatment of Cu/SiO$_2$ and Cu/ZnO/Al$_2$O$_3$ the samples were pre-reduced by the normal treatment, then exposed to a 50 NmL/min flow of 100% H$_2$ at 523 K for 1 hour. Finally the flow was switched to 79 Nml/min of 9.5% CO (balanced in Ar) and heated with 5 K/min to 573 K and kept constant for 30 minutes before thorough He purge at 573 K to remove residual and adsorbed CO and cooling in He to 276 K where adsorption of 0.4 mbar CO was conducted.

For experiments with deposition of formate on Cu/ZnO or Cu/SiO$_2$, the pre-reduced sample was flushed and cooled in He to 373 K (atmospheric pressure), where it was exposed to CO$_2$/N$_2$/H$_2$ (3/29/68) flow until stable IR signals before cooling to 276 K in the syngas mixture. A background spectrum was recorded in He at 276 K and used for recording spectra (in Kubelka-Munk units) during a subsequent exposure to 0.4 mbar CO. After CO adsorption, the sample was thoroughly flushed with He at 276 K before performing a TPD in 45 Nml/min He with a heating ramp of 10 K/min to 323 K before further heating by 2 K/min to a final temperature of 393 K with a dwell time of 5 min. During cooling from the final TPD temperature, a 10 min dwell step at 353 K in a 150 Nml/min He flow was included to prevent re-adsorption of desorbed adsorbates. The higher He flow was maintained during further cooling to 276 K, where a new background spectrum was

Table 1

Results from structural characterization of the reduced samples by N₂O-RFC and in situ XRD.

Sample	Nominal Cu content [wt %]	Cu surface area [m^2 Cu/g$_{cat}$]	Cu crystallite size from XRD [nm] [a]	Cu diameter from Cu surface area [nm]
Cu/SiO₂	10	3.99	67.3	16.8
Raney Cu	98.9	5.18	40.7	47.5 [b]
Cu/Al₂O₃	20	4.80	2.9	28.0
Cu/TiO₂	20	1.19	65.7	112.9
Cu/ZnO	10	4.90	3.9	13.7
Cu/ZnO/Al₂O₃	63	20.25	4.7	20.9

[a] Determined based on the Cu {111} diffraction peak at 43.1° (ICSD cc. 64699) after activation.

[b] Determined from the combination of the free Cu area and the Al₂O₃ covered surface area determined by Nielsen et al. [34].

collected for the subsequent CO adsorption exposure. The combined TPD and CO adsorption cycle was repeated with increased final TPD temperature in steps of 20 K (413 K, 433 K and 453 K).

To evaluate the effects of sample dilution with KBr, which has been used for many similar studies in the literature, measurements were conducted with the Cu-based samples physically mixed with KBr. The KBr-sample mixture was then subjected to the same pre-reduction and measurement protocols used in the standard experiments and analyzed by IR measurements on chemisorbed CO.

3. Results and discussion

3.1. Sample properties

The results from structural characterization of the samples are summarized in Table 1. Details of the post reduction XRD patterns are shown in the supplementary material Figs. S1-S7. The constant angle (2θ) of the XRD reflections from Cu for all the samples (see Fig. S7b) suggests that bulk alloying of Cu and support components do not occur for any of the samples with the applied reduction methods. Precipitated samples (Cu/Al₂O₃, Cu/ZnO/Al₂O₃, Cu/ZnO, Cu/TiO₂) have a smaller crystallite size than the Cu diameter determined from the Cu surface area. This suggests that the samples are polycrystalline with larger particles composed of smaller crystallites. However, an extent of decoration of the metal particles (i.e. an "iceberg" configuration) by the support can also contribute to an overestimate of the Cu particle size relative to the XRD crystallite size estimates. Oppositely, Cu/SiO₂ prepared by impregnation exhibits a larger crystallite size than the size determined from the surface area. This has also been observed previously [42] for Cu/SiO₂ prepared by impregnation. The impregnation method must have resulted in larger crystallites that dominate the XRD measurement over a majority of smaller particles that dominate the Cu area. For Raney Cu the size estimates from XRD and chemisorption are similar, indicating that the sample consists of relatively homogeneous 40-50 nm Cu crystals. Previous characterization [34] has shown that around 30-40% of the surface of these crystals is free metallic surface, whereas the rest is covered with a thin Al₂O₃ film.

It is known that the TOF for methanol synthesis over Cu based samples (and hence expectedly the surface properties) is generally size-independent for Cu particles larger than ca. 5 nm [12,43,44]. Xu and Goodman [45] also found that the IR spectrum of CO adsorbed on a Cu/SiO₂ model system became relatively size-independent above ca. 3.5 nm in diameter (below 30% Cu dispersion). The surface properties should therefore be relatively constant for particle sizes above the limit of 3.5-5 nm. As the crystallite sizes are close to or above this limit (Table 1), and as the area-derived particle sizes are well above this limit, it is unlikely that the present comparisons across supports are affected by differences in particle size.
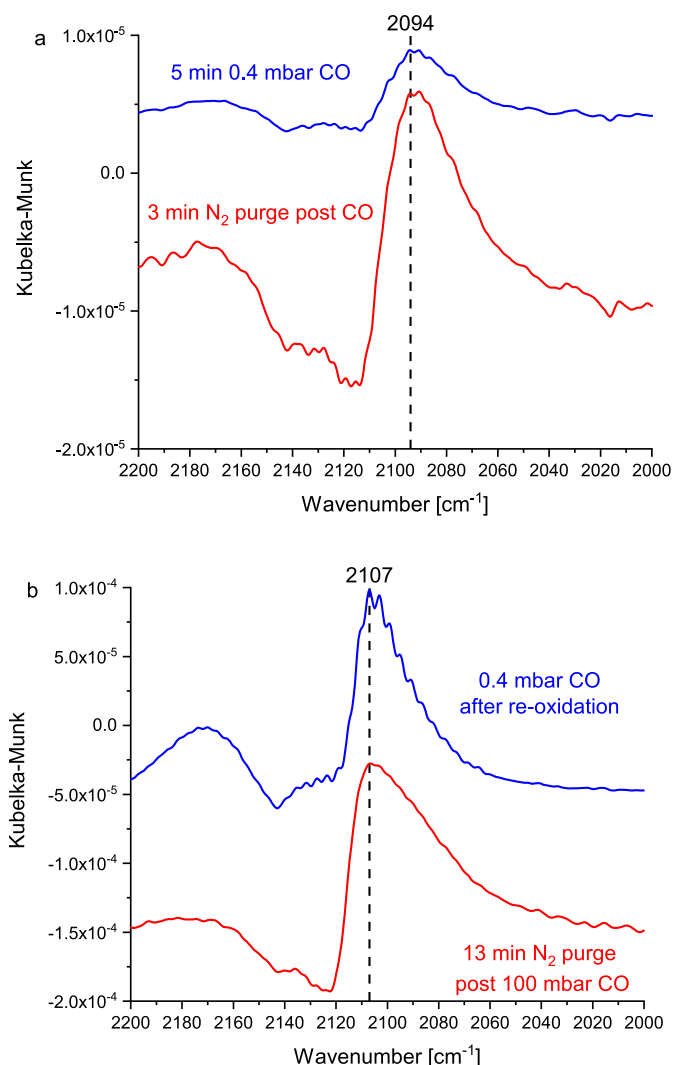
Fig. 2. a) IR spectra of pre-reduced Raney Cu in the presence of 0.4 mbar CO (blue) and after subsequent N₂ purge (red) both at 153 K. b) IR spectra of pre-reduced and then re-oxidized (by 9% CO₂/N₂ at room temperature) Raney Cu in 0.4 mbar CO at 152 K and during N₂ purge at 152 K post stepwise increase in CO pressure from 0.4 mbar to 100 mbar CO.

3.2. Raney Cu

A previous study [34] with the same Raney Cu sample evaluated the catalytic properties and showed that Raney Cu featured the intrinsic properties of Cu. Consequently, CO adsorption on Raney Cu should be representative of the intrinsic properties of Cu in the absence of notable support effects. Spectroscopic measurements on metal-rich Cu samples are complicated by the high reflectance of the metal [16], which is the most likely reason, why only weak signals were obtained in the present DRIFTS experiments on Raney Cu. The measurements were therefore conducted at low temperature, where adsorbed CO can be preserved for some time after purging the cell of gaseous CO. This allows a clearer identification of the band from adsorbed CO.

Fig. 2a shows the IR spectrum of pre-reduced Raney Cu during CO adsorption at 153 K and after a subsequent 3 min N₂ purge until only minor traces of gaseous CO could be detected. The IR band at 2094 cm^{-1}, which is preserved during removal of gaseous CO, is attributed to adsorbed CO on metallic Cu. Comparison to single crystal studies [16,46] suggests that this spectrum is dominated by the contribution from the (110) facets. Previous [47–49] Wulff-construction modeling on Cu has yielded a distribution of 5-7% (110), 25-30% (100), and 60-70% (111) for the Cu surface. The catalytic properties of the Raney Cu

sample are also relatively similar to those of a Cu(111) single crystal surface [34], which supports that this equilibrium distribution is representative for the present Raney Cu sample. It could thus seem contradictory that the least abundant facet dominates the spectrum in Fig. 2a, but this can be rationalized from the dipole coupling effects mentioned in the introduction. Single crystal studies [16,46] show that the C-O frequency decreases in the order (110) > (100) > (111). As the interference phenomena from dipole coupling strongly favor the higher C-O frequency sites, the contribution from higher frequency (110) sites dominates the spectrum despite representing a minority of the surface sites. The strong effects of dipole coupling seen for the Raney Cu reference suggests that polycrystalline Cu samples generally must be expected to be dominated by the higher frequency contributions, such as Cu(110), despite the limited concentration of such sites.

Fig. 2b shows the IR spectrum of the adsorbed CO on Raney Cu that had been first pre-reduced and then re-oxidized by 9% CO_2/N_2 at room temperature. Fig. 2b illustrates that this yields a C-O band at 2107 cm^{-1} in the frequency range indicative of CO on oxidized Cu^+ sites (Fig. 1). The fact that the 2094 cm^{-1} band seen for the reduced sample is replaced with a higher frequency band by the oxidative treatment helps to verify that the 2094 cm^{-1} band is due to CO adsorption on metallic Cu.

3.3. Cu/Al$_2$O$_3$

Fig. 3a shows the IR spectrum for CO adsorbed at 276 K on pre-reduced Cu/Al$_2$O$_3$ with a main band located at 2089 cm^{-1} attributed to CO on the metallic surface on the basis of a comparison to Fig. 1. Fig. 3b shows the IR spectrum for CO adsorbed at 276 K on pre-reduced and then re-oxidized (9% CO_2/N_2 at room temperature) Cu/Al$_2$O$_3$, which shows a main band at 2109 cm^{-1} indicative of CO on relatively well-developed Cu^+ sites (Fig. 1). Since the 2089 cm^{-1} band seen for reduced Cu/Al$_2$O$_3$ is significantly displaced by the oxidative treatment (Fig. 3), and because D'Alnoncourt et al. [50] observed that more severe reduction of Cu/Al$_2$O$_3$ did not change this band substantially, the 2089 cm^{-1} band is attributed to the metallic Cu surface. If the partially oxidized sample is exposed to increasing CO pressures the band also seems to shift down towards the metallic state (Fig. S8).

Table 2 compares the presently achieved C-O frequency to values reported for reduced Cu/Al$_2$O$_3$ in the literature. Generally the results agree within a few cm^{-1}, which would suggest that measured C-O frequencies are reproducible to the extent that even small variations are significant.

3.4. Cu/TiO$_2$

Arakawa et al. [53] investigated methanol synthesis catalyzed by Cu/TiO$_2$ and concluded that the turnover frequency per exposed metallic Cu atom was high. TiO$_2$ is thus an example of a support that can exert a clear support effect on Cu that in methanol synthesis causes a high turnover frequency. Fig. 4 shows IR spectra as a function of time when pre-reduced Cu/TiO$_2$ is exposed to 0.4 mbar CO at 276 K. This clearly illustrates the existence of two IR bands at 2070 cm^{-1} and 2104 cm^{-1}. These bands are attributted to CO adsorbed on Cu sites, since adsorption on TiO$_2$ yields higher C-O frequencies [54].

Fig. 5a shows that the 2070 cm^{-1} band is displaced more rapidly than the 2104 cm^{-1} band when the IR cell is flushed with He at 276 K after CO adsorption. Given that CO is bound more strongly to Cu^+ sites [29] this could indicate that the higher frequency 2104 cm^{-1} band is due to more strongly bound CO on $Cu^{\delta+}$ sites at $Cu^{\delta+}$-O-Ti linkages to the support, whereas the lower frequency 2070 cm^{-1} band is due to more weakly bound CO on the metallic surface. This assignment is strongly supported by Fig. 5b, which shows the spectrum of CO adsorbed on the air calcined, CuO/TiO$_2$ oxide precursor and illustrates that the high-frequency band is very prominent for the oxidized state of the sample. Oppositely, the low-frequency band is absent in the
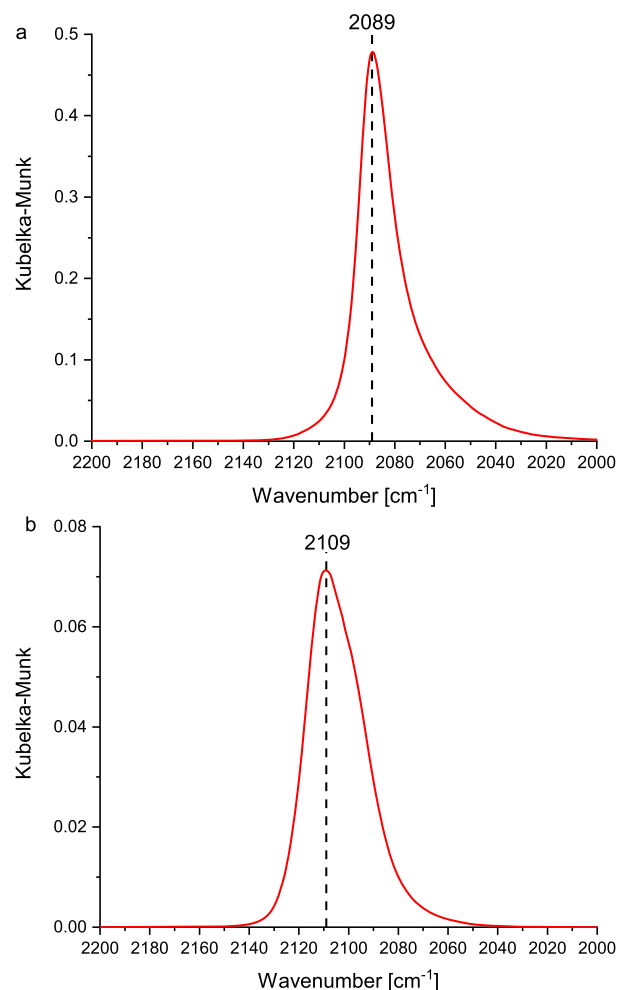
Fig. 3. a) IR spectrum of pre-reduced Cu/Al$_2$O$_3$ in 0.4 mbar CO at 276 K. b) IR spectrum of pre-reduced and then re-oxidized (in 9% CO_2/N_2) Cu/Al$_2$O$_3$ in 0.4 mbar CO at 276 K.

Table 2
Measured ν_{C-O} for CO adsorption on reduced Cu/Al$_2$O$_3$ in this study and comparison to studies in the literature. None of the studies from the literature mention any sample dilution by KBr.

Study	Reference	Cu content [wt%]	ν_{C-O} on metallic Cu [cm^{-1}]
Topsøe and Topsøe	[30]	2.5	2094
D'Alnoncourt et al.	[50]	20	2090
Padley et al.	[51]	5	2094
Dulaurent et al.	[52]	4.7	2092
This work		20	2089

oxidized sample. Consequently, the 2104-2106 cm^{-1} high-frequency band is attributed to CO on $Cu^{\delta+}$-O sites linked to the TiO$_2$ oxide matrix, whereas the 2070 cm^{-1} band is attributed to CO on the metal surface.

The significantly lower C-O frequency on the metal surface of Cu/TiO$_2$ compared to the Raney Cu reference suggests that the Cu surface in Cu/TiO$_2$ is significantly modified by the support. Dipole coupling makes it likely (see section 3.2) that the main contribution from the metallic surface (2070 cm^{-1} for Cu/TiO$_2$) arises from the sites such as the (110) facet that yield considerably higher frequencies on unperturbed single crystal surfaces [16,46]. Considering the charge-frequency relationship in Fig. 1 the low frequency on Cu/TiO$_2$ indicates a negative charging of the Cu surface. At the interface between a metal and an n-type semiconductor such as TiO$_2$ there will be a charge
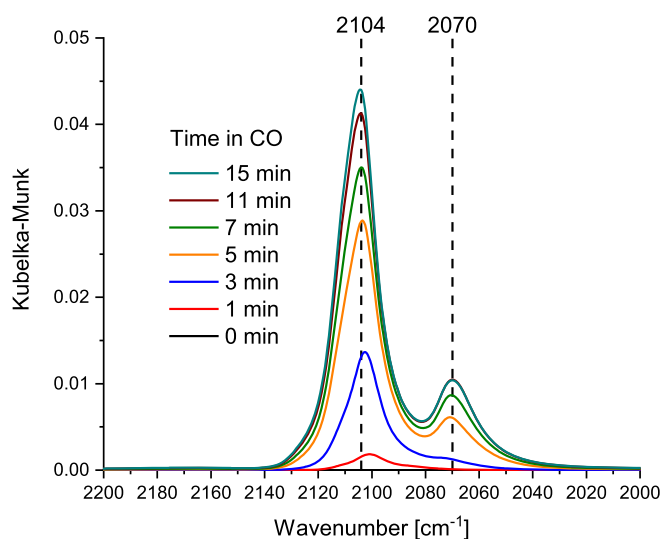
Fig. 4. IR spectra of pre-reduced Cu/TiO_2 as a function of time during exposure to 0.4 mbar CO at 276 K.
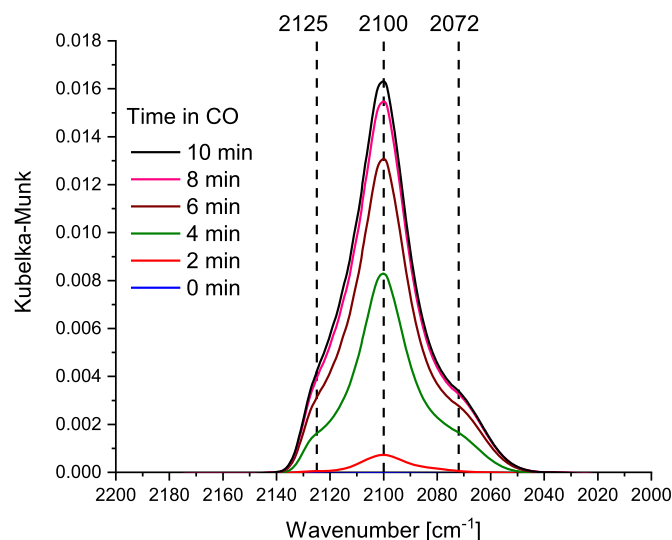

Fig. 6. IR spectra of pre-reduced Cu/SiO_2 as a function of time during exposure to 0.4 mbar CO at 276 K after normal pre-reduction (5% H_2 at 523 K).
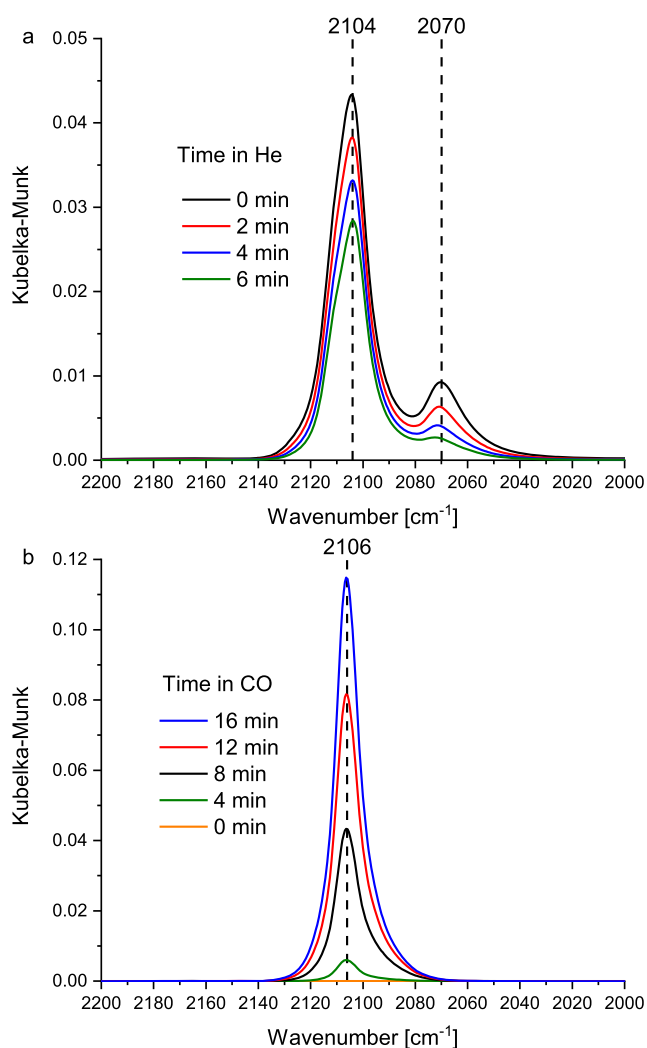

Fig. 5. a) IR spectra of pre-reduced Cu/TiO_2 as a function of time during He flush after exposure to 0.4 mbar CO at 276 K. b) IR spectra of fresh, air calcined CuO/TiO_2 as a function of time during exposure to 0.4 mbar CO at 276 K. Fig. S4 shows that the oxidized sample contains a mixture of CuO and Cu_2O phases.

transfer from the semiconductor to the metal [55–57]. In the classical limit, charge transferred to a conductor, such as the copper metal, is distributed across the surface, and DFT calculations suggest that this behavior of charge distribution across the surface is emerging already in very small metal clusters [58]. Such charge transfer effects can ratio-nalize the negative charging of the Cu surface on the n-type semi-conductor supports including TiO_2.

3.5. Cu/SiO₂

Fig. 6 shows time-resolved spectra during CO adsorption at 276 K on pre-reduced Cu/SiO_2 dominated by a central 2100 cm^{-1} band with two shoulders at approximately 2072 cm^{-1} and 2125 cm^{-1}. The present spectra are similar to those of lower Cu-dispersion (< 30%) Cu/SiO_2 model systems in UHV experiments [45], which suggests that the cur-rent measurements are free of experimental artifacts such as gas phase impurities.

The multiple IR bands for the reduced Cu/SiO_2 sample raises the question of which bands that arise from the metallic surface. Fig. 7a shows the spectrum of CO adsorbed on the freshly calcined CuO/SiO_2 oxide precursor, where the high-frequency band (2127 cm^{-1}) is clearly present. Fig. 7b shows comparisons between CO adsorbed on pre-re-duced Cu/SiO_2 and on pre-reduced and then re-oxidized (by 9% CO_2/ N_2 at room temperature) Cu/SiO_2. The figure reveals that oxidative treatment strengthens the high-frequency band and eliminates the two lower frequency bands. These results clearly show that the band at 2125-2127 cm^{-1} is from oxidized Cu^+ sites. In the reduced sample the remnant of such species are most likely the Cu^+-O-Si linkages at the metal/oxide interface. Oppositely, the two lower frequency bands are attributed to CO adsorption on the metallic surface. The 2100 cm^{-1} band is thus the main band from the metallic surface, which from analogy to the Raney Cu results is expected to be the higher C-O fre-quency facets, particularly Cu(110), that are strengthened by dipole coupling. The shoulder towards lower frequency is most likely from the more densely packed facets that are disfavored by the dipole coupling, but nevertheless slightly visible due to the good resolution achieved in spectra for Cu/SiO_2. During flushing of the cell with He the bands from adsorbed CO disappear with similar rates (Fig. S9). There are thus no clear differences in binding strength to aid the band assignment.

The main CO band attributable to the metallic surface of Cu/SiO_2 is thus shifted upwards by 6 cm^{-1} compared to Raney Cu and is between the frequencies observed on reduced and oxidized Raney Cu (see Fig. 2). Considering the discussion in section 3.3 this shift is most likely
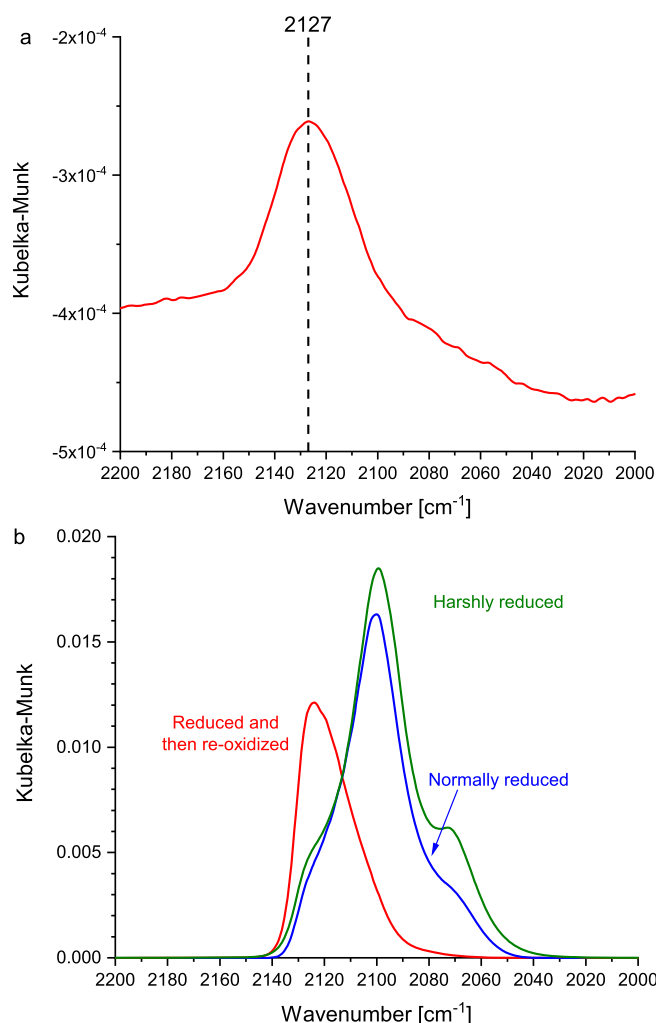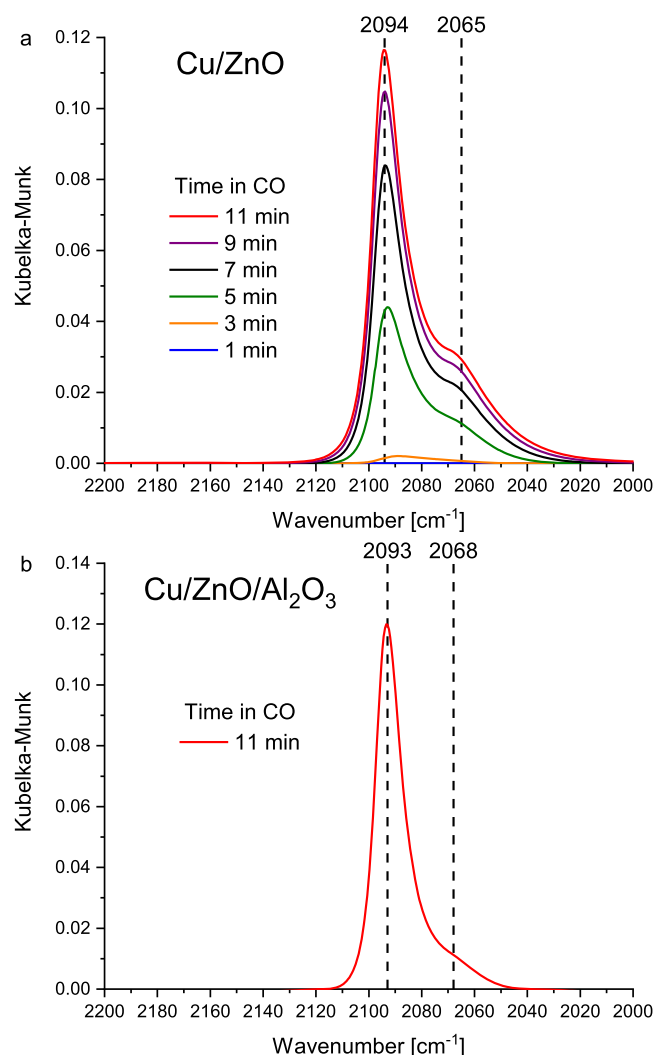
Fig. 7. a) IR spectrum of freshly calcined CuO/SiO$_2$ after pre-adsorption of 0.4 mbar CO at 276 K followed by 16 min He purge at 276 K. b) IR spectra during exposure to 0.4 mbar CO at 276 K for normally pre-reduced (blue), harshly pre-reduced by 9.5% CO at 573 K (green) and normally pre-reduced and then re-oxidized (9% CO$_2$/N$_2$ at room temperature, red) Cu/SiO$_2$.

Fig. 8. IR spectra of pre-reduced a) Cu/ZnO in 0.4 mbar CO at 276 K and b) Cu/ZnO/Al$_2$O$_3$ in 0.4 mbar CO at 276 K.

of sufficient magnitude to represent a significant difference. From the charging-frequency relationship in Fig. 1 the higher frequency on Cu/SiO$_2$ indicates that the surface of Cu particles on silica is electron depleted. The most likely reason for this depletion is that the Cu$^+$-O-Si linkages observable in the spectrum are so electron-withdrawing that the whole Cu surface becomes slightly electron deficient.

3.6. Cu/ZnO based samples

Cu/ZnO/Al$_2$O$_3$ is the industrial catalyst for methanol synthesis, and it is well-substantiated that ZnO exerts a strong beneficial support effect [9–13]. Cu/ZnO based catalysts with or without alumina have been observed [13] to exhibit similar turnover frequencies for methanol synthesis and are discussed together in this section. Fig. 8a shows the IR spectrum of Cu/ZnO in presence of 0.4 mbar CO at 276 K, whereas Fig. 8b displays the spectrum of Cu/ZnO/Al$_2$O$_3$ in 0.4 mbar CO at 276 K.

In good agreement with previous studies [30,50,59] the Cu/ZnO (/Al$_2$O$_3$) samples show two IR absorption bands centered at 2093-2094 cm^{-1} and at 2065-68 cm^{-1} with the lower frequency band being more clear in Cu/ZnO. Any contribution from CO adsorbed on ZnO is excluded, as this occurs around 2190 cm^{-1} [60,61]. Fig. S10 shows the development in the spectrum of adsorbed CO at various stages during

the reduction of Cu/ZnO/Al$_2$O$_3$ and illustrates that a band at 2100 cm^{-1} on the initial oxidized state is replaced by the spectrum characteristic of the reduced sample at 448 K.

As touched upon in the introduction band assignments can be particularly difficult on basic oxides, where Cu$^{\delta+}$ sites from Cu-O linkages to the support may yield C-O frequencies similar to the Cu$^{\delta+}$ sites seen at protrusions in an unperturbed metallic surface. Previous studies [31,62] on Cu/ZnO(/Al$_2$O$_3$) samples report that the high frequency band can be eliminated by harsher reduction in CO-containing gas. This could indicate that the high-frequency band arises from an oxidized species. However, we were unable to reproduce this elimination of the 2093-2094 cm^{-1} band by harsher reduction (Fig. 9a), although the reason for this discrepancy is not completely clear. Fig. 9b shows IR spectra at various CO pressures and during subsequent flushing in He for a Cu/ZnO/Al$_2$O$_3$ sample that has been pre-reduced and then re-oxidized (9% CO$_2$ at room temperature). Fig. 9b illustrates that the oxidized sample exhibits a broad band around 2100 cm^{-1}. The fact that the major band is at relatively similar frequencies for both the reduced and oxidized sample (compare Figs. 9a and 9b) could indicate that this band arises from oxidized sites, such as Cu-O-Zn linkages to the support. Additionally, the high frequency band is relatively more stable when the gaseous CO is flushed away with He (Figs. 9b and S11), whereas the shoulder at 2065-2068 cm^{-1} is displaced more easily (Fig. S11). This could also suggest that the lower frequency shoulder represents the
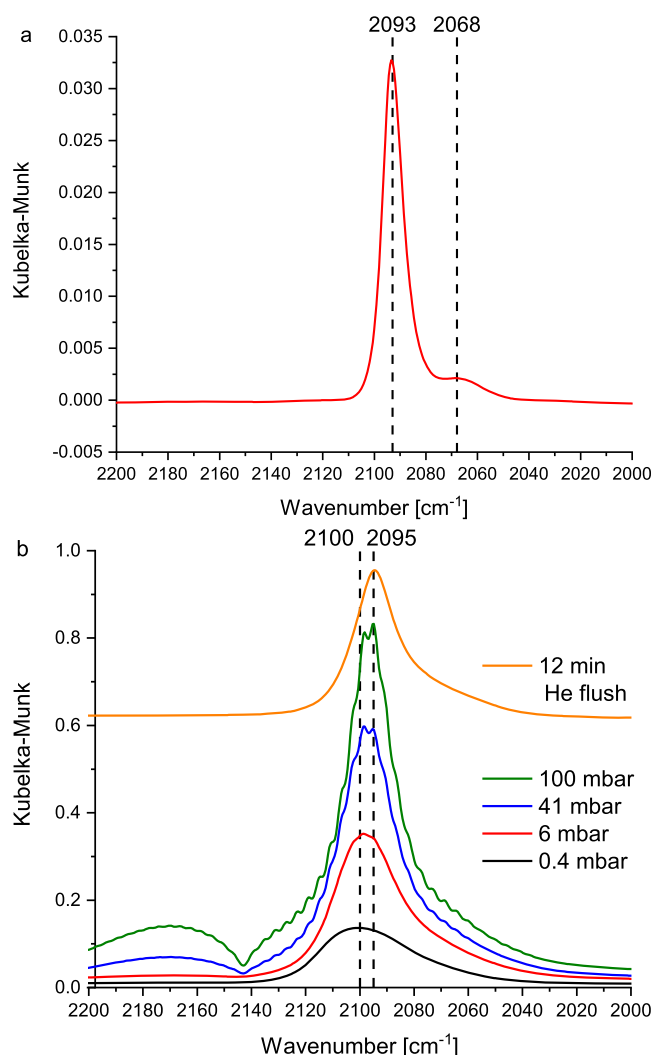
Fig. 9. a) IR spectrum of Cu/ZnO/Al$_2$O$_3$ in 0.4 mbar CO at 276 K after harsh pre-reduction with 30 minutes in 9.5% CO/Ar at 573 K after the normal pre-reduction. b) IR spectra of pre-reduced and then re-oxidized (by 9% CO$_2$/N$_2$ at room temperature) Cu/ZnO/Al$_2$O$_3$ in 0.4 mbar to 100 mbar CO and during subsequent He flush at constant 276 K. Spectra are offset for clarity.

more weakly bound CO on the metallic surface, whereas the high-frequency represents stronger bonding on oxidized sites.

Based on these observations it is most likely that the 2093-2094 cm^{-1} main band is part of the reduced particles, since it cannot be modified by hasher reduction (Fig. 9a). However, given the similarity to the main band on an oxidized sample (Fig. 9b) it is also likely that the 2093-2094 cm^{-1} band represents a partially oxidized site, namely the Cu$^{\delta+}$-O-Zn sites at the periphery of the metal particle. The 2065-68 cm^{-1} band is assigned to the CO adsorbed on the interior metallic surface. Chemisorption techniques [63] suggest that there are relatively few Cu-O-Zn sites compared to metallic Cu^0 sites in reduced Cu/ZnO (/Al$_2$O$_3$). If the 2093-2094 cm^{-1} band is due to Cu$^{\delta+}$-O-Zn sites its high intensity must therefore arise from dipole coupling.

Both Cu/SiO$_2$ and Cu/ZnO(/Al$_2$O$_3$) show some similarities in the CO spectra with a main peak in the 2090-2100 cm^{-1} range and a shoulder towards lower frequency. However, as outlined above different band assignments are applied for the two systems with the most intense band assigned to the metallic surface for Cu/SiO$_2$ and to a site linked to the oxide matrix for Cu/ZnO(/Al$_2$O$_3$). The main argument for this interpretive difference comes from the supporting studies of oxidized samples, where oxidized Cu sites for Cu/ZnO(/Al$_2$O$_3$) appears to be at a

considerably lower frequency (ca. 2100 cm^{-1} in Fig. 9b) than the oxidized Cu sites for Cu/SiO$_2$ (2125-2127 cm^{-1} in Fig. 7). However, the complex analysis induced by dipole coupling, where the most intense IR bands may arise from the most coupling-favored high-frequency sites rather than from the most physically abundant sites must be remembered in these interpretations.

Cu single crystal studies [16,46] have not shown frequencies below 2070 cm^{-1}, so the observation of a lower frequency feature for Cu/ZnO (/Al$_2$O$_3$) indicates a negative charging of the metallic surface (see Fig. 1). This would also be consistent with the observation of a low-frequency feature for Cu/TiO$_2$ (see section 3.4) given that both TiO$_2$ and ZnO are n-type semiconductors. Additionally, Behm and co-workers [64] inferred from the C-O frequency in CO adsorbed on Au/ZnO that the surface of gold dispersed on ZnO is negatively charged. Prior XPS analyses [65,66] of Cu/ZnO are also consistent with a negative charging of the Cu surface. The conclusion of a negative charging on the Cu surface of Cu/ZnO(/Al$_2$O$_3$) is therefore supported by other techniques/systems.

### 3.7. Effect of formate decoration of the metal surface

The main band for Cu/SiO$_2$ (2100 cm^{-1}) is between bands seen on the reduced and oxidized states of the Raney Cu reference, which could suggest a charge depletion of the metal surface in Cu/SiO$_2$. Oppositely the n-type semiconductor supports ZnO and TiO$_2$ yield low-frequency features that may indicate an increased negative charge in the Cu surface. It is therefore relevant to validate, if the observed bands indeed are due to adsorption on copper sites. This was examined in experiments involving formate deposition on copper. It is known from single crystal studies [67] that a sufficiently high coverage of formate can partially or completely exclude the CO adsorption on copper, and that pre-adsorbed formate on Cu can be removed by TPD to 450 K [34], whereas desorption of formate on ZnO occurs at higher temperatures [68–70]. The Cu surface of a HCOO covered sample can thus be selectively exposed by heating to temperatures up to 450 K, where only the formate on Cu desorbs.

Formate was adsorbed on pre-reduced Cu/ZnO and Cu/SiO$_2$ by CO$_2$/N$_2$/H$_2$ (3/29/68) exposure (373 K, 1 atm.). Fig. 10 shows the IR spectra in He at 276 K for the two samples after the CO$_2$/H$_2$ treatment. Fig. 10a shows that the exposure of Cu/ZnO to CO$_2$/H$_2$ resulted in distinct HCOO features on both Cu [71–73] ($\nu_{OCO,sym}$ = 1352 cm^{-1}, $\nu_{OCO,asym}$ = 1602 cm^{-1} and ν_{H-C} = 2852 cm^{-1}) and ZnO [72,74] (2882 cm^{-1}, 1580 cm^{-1}) as well as CH$_3$O-ZnO [72] (2931 cm^{-1}) and zinc-related bicarbonate species [74] (1305 cm^{-1}). For Cu/ZnO the C-H features are clearer in the raw absorbance spectrum in Fig. S12, which also shows a broad IR absorbance across the entire spectrum attributable to light absorption from intraband excitations of free charge carriers in the ZnO conduction band [75–77]. Fig. 10b shows that the exposure of Cu/SiO$_2$ to CO$_2$/H$_2$ resulted in Cu-HCOO ($\nu_{OCO,sym}$ = 1352 cm^{-1}) and features at 2934 cm^{-1} and 2852 cm^{-1} that may arise from either Cu-HCOO or CH$_3$O-SiO$_2$ [78–80].

After decoration of the Cu surface with HCOO (Fig. 10) the spectrum of adsorbed CO on the maximally HCOO covered sample was measured in 0.4 mbar CO at 276 K with the result displayed in Fig. 11. A series of TPD sequences were then conducted. Here the sample was heated in He to progressively higher temperatures to desorb increasing amounts of the adsorbed formate. The gradual desorption of formate during the TPD runs was verified by the progressive disappearance of the Cu-HCOO IR features (Figs. S13 and S14) and by the concurrent detection of H$_2$ and CO$_2$ in the effluent during the TPDs (Figs. S15 and S16). After each TPD sequence the sample was cooled and subjected to 0.4 mbar CO adsorption at 276 K, where the IR spectrum for CO adsorption was recorded. Fig. 11 summarizes the CO spectra at 276 K recorded between the TPD sequences for both Cu/ZnO and Cu/SiO$_2$.

The first conclusion to be drawn from Fig. 11 is that the observed IR bands are due to CO adsorption on copper sites, as they can be
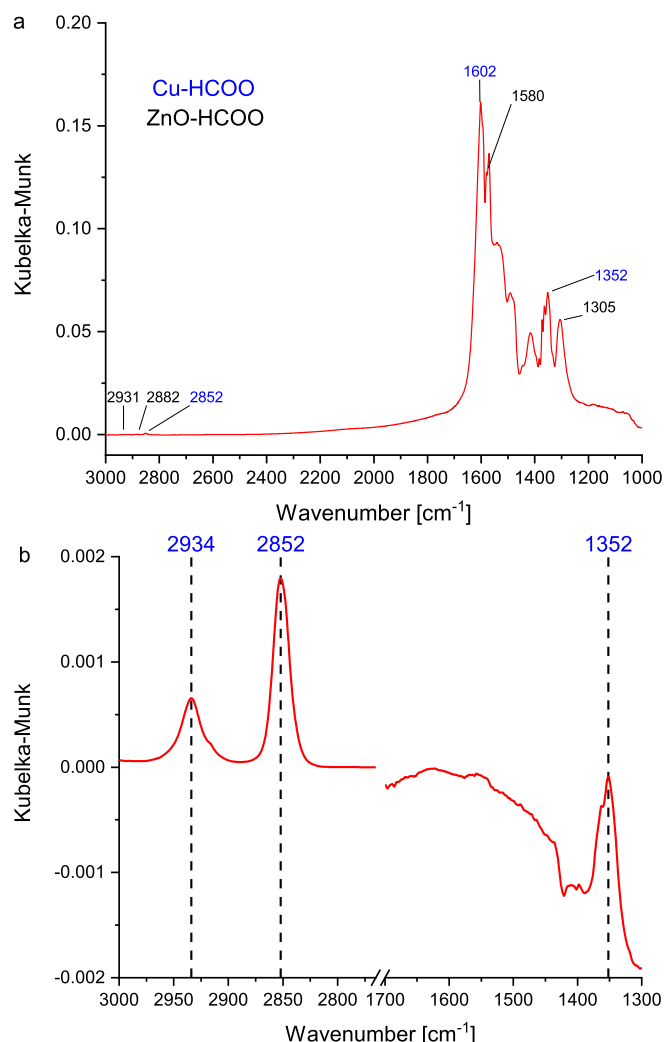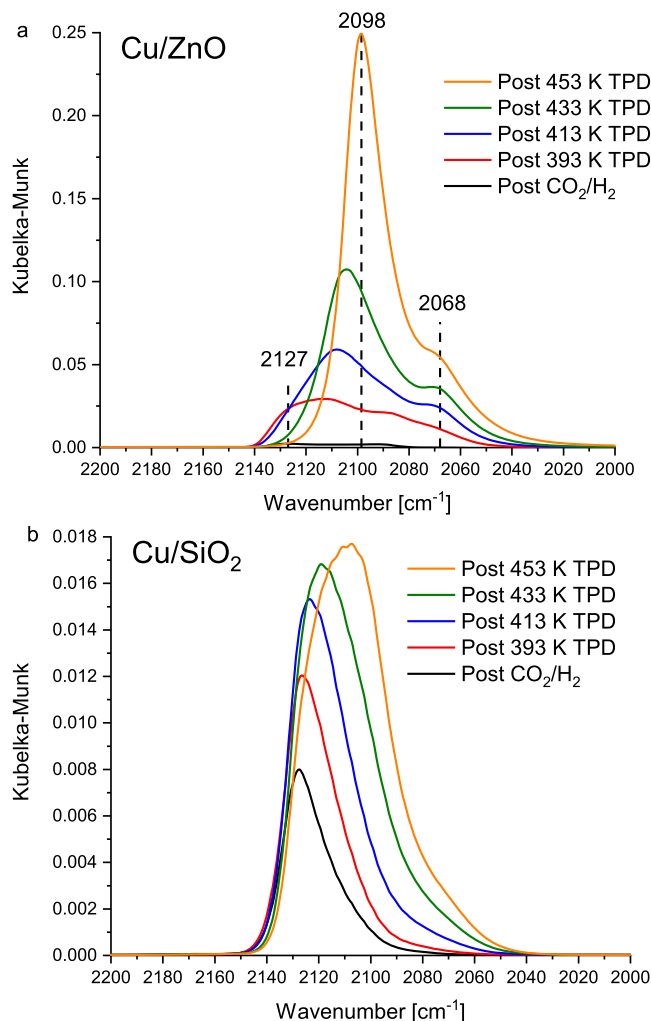
Fig. 10. a) IR spectrum of Cu/ZnO in He at 276 K HCOO bands after $CO_2/N_2/H_2$ (3/29/68) exposure at 373 K, atmospheric pressure. Cu and ZnO related species are marked in blue and black, respectively. See Fig. S12 for a clearer view of the bands above 2700 cm^{-1}. b) IR spectrum of pre-reduced, and HCOO covered Cu/SiO$_2$ in He at 276 K with Cu-HCOO bands after $CO_2/N_2/H_2$ (3/29/68) exposure at 373 K, atmospheric pressure.

Fig. 11. IR spectra in 0.4 mbar CO at 276 K for a) Cu/ZnO and b) Cu/SiO$_2$. The measurements are conducted after formate decoration of the samples by CO_2/H_2 treatment and after consecutive TPDs in He to increasingly higher temperatures. Each background is the partly HCOO-covered sample prior to each CO adsorption. The HCOO covered state in Fig. 10 is thus the background for the "Post CO_2/H_2" spectrum here. See Fig. S17 for a detailed view of the very weak "Post CO_2/H_2" spectrum for Cu/ZnO.

displaced by HCOO blockage of the Cu surface and fully restored by TPD to 453 K, which is known [34] to desorb all formate from Cu. The formate species associated with zinc are essentially preserved during the TPD (Fig. S13 and S14), and as such sites thus remain blocked during the experiment in Fig. 11a, it can be ruled out that the observed CO bands are associated with zinc-species.

The differences between these two identically treated samples also provide important insight into the support effect upon the Cu surface. Cu/ZnO facilitates a relatively high formate coverage on Cu resulting in a completely physically filled Cu surface as evident from the nearly complete absence of CO uptake for Cu/ZnO after H_2/CO_2 treatment ("Post CO_2/H_2" in Fig. 11a). Oppositely Cu/SiO$_2$ (Fig. 11b) shows a clear CO band already at the maximal HCOO coverage after CO_2/H_2 treatment. It is also a striking difference that Cu-HCOO on Cu/ZnO exhibits an asymmetric OCO stretch at 1602 cm^{-1} (Fig. 10a), which is completely absent in Cu/SiO$_2$ (Fig. 10b). This asymmetry could be due to the higher formate coverage on the Cu surface of Cu/ZnO that causes the formate molecules to tilt to accommodate neighbors in close proximity as observed in single crystal studies [67,81].

Several techniques [49,82–85] have shown that adsorbed formate is an electron-withdrawing species. With the highest coverage of electron-

withdrawing formate Cu/ZnO features two main bands from adsorbed CO at 2098 cm^{-1} and 2127 cm^{-1} (Fig. 11a and more clearly in Fig. S17). As the HCOO coverage gradually decreases by the TPD treatments these CO bands progressively shift to 2068 cm^{-1} and 2098 cm^{-1}, close to the positions for a freshly reduced sample (Fig. 8a). Similar gradual frequency shifts are seen as formate desorb from Cu/SiO$_2$. Weak van der Waals interactions between adsorbed HCOO and CO are ruled out as an explanation for these frequency shifts. This is because there are no matching changes in the C-H and OCO regions of the spectrum to indicate distortion of the formate by the CO adsorption (Figs. S18-S20). Consequently, the frequency changes in adsorbed CO with the amount of co-adsorbed formate must reflect that the charging state of Cu surface sites not occupied by formate is modified by the amount of electron-withdrawing adsorbates.

These observations suggest that the Cu surface of Cu/ZnO is able to donate charge to the adsorbed formate to the extent that it ensures a complete physical filling of the Cu surface. By contrast the Cu surface of Cu/SiO$_2$ is only able to support a formate coverage until the point where the remaining Cu surface becomes charge depleted to a degree (evident from a high C-O frequency in the co-adsorbed CO in Fig. 11b) that it is unable to sustain additional formate. This suggests that

Table 3
Measured $\nu_{C\text{-}O}$ associated with metallic Cu on various pre-reduced Cu samples during CO adsorption at 276 K (Raney Cu at 153 K).

Sample	$\nu_{C\text{-}O}$ for the primary band attributed to the metallic surface [cm^{-1}]	$\nu_{C\text{-}O}$ for Cu$^{\delta+}$ [cm^{-1}]
Cu/SiO$_2$	2100	2125-2127
Raney Cu	2094	2107
Cu/Al$_2$O$_3$	2089	2109
Cu/TiO$_2$	2070	2104-2106
Cu/ZnO(/Al$_2$O$_3$)	2065-2068*	2093-2100

* Band assignments are challenging as discussed in Section 3.6. Here it is assumed that the 2093-2094 cm^{-1} band is from Cu-O linkages to the support and not due to sites on the interior metallic surface.

adsorbates such as formate are able to accomodate the surface charge in the metal-adsorbate bonding. It would be consistent with a support-induced negative charging of the metal surface in Cu/ZnO that the metal surface is able to donate more charge to the adsorbates resulting in a higher formate coverage.

The role of surface charging in governing the interaction with electron-withdrawing adsorbates is potentially important for the catalytic properties, as some of the important Cu-catalyzed reactions involve electron-withdrawing adsorbates. This includes formate in the synthesis of methanol [34,70,86] and adsorbed oxygen in the water-gas shift reaction [87–89].

3.8. CO stretching frequencies on supported Cu

Table 3 summarizes the C-O frequency for the main band attributed to the metallic Cu surface and to oxidized Cu$^{\delta+}$ sites for each sample and shows a clear variation in the C-O frequency with the choice of support. For the ZnO-free supports the values for the metallic surface in Table 3 represent the most intense band that is not also present in the oxidized sample. For the ZnO-containing samples the interpretation is more difficult and we have tentatively assigned the lower-frequency feature as the major feature from the metallic surface.

The previously discussed consistency among the reported C-O stretches for Cu/Al$_2$O$_3$ (Table 2) underlines that even small change to the C-O stretch are potentially significant. Figs. 4, 6, and 8 show that the rising intensities (and hence rising CO coverage) as a function of time during CO dosage indicate no substantial shifts in frequencies. This suggests that the coverage dependence of the frequencies is too weak to distort a comparison across the various samples. As discussed in section 3.1 the samples also have Cu crystallite/particle sizes that are close to or above the size where the Cu surface properties become size insensitive. Furthermore there is no correlation between frequencies and XRD crystallite size or area derived particle size as illustrated in Fig. S21 in the supporting information. Structure sensitivity can therefore not account for the changes in the C-O stretches across the samples. Hence the frequency shifts in Table 3 must arise from support effects.

It has been common to interpret the support dependence of the C-O frequency in terms of a preferential faceting by comparison to the most similar single crystal results. By such an interpretation Cu/Al$_2$O$_3$ ($\nu_{C\text{-}O}$ = 2089 cm^{-1}) should be dominated by Cu(100) facets, as a Cu(100) single crystal gave $\nu_{C\text{-}O}$ = 2088 cm^{-1} at a very similar CO pressure [90]. Cu/SiO$_2$ ($\nu_{C\text{-}O}$ = 2100 cm^{-1}) should be dominated by Cu(311) facets considering the observation [16] of $\nu_{C\text{-}O}$ = 2093-2104 cm^{-1} on a Cu(311) single crystal. However, such an interpretation is unlikely to be correct for two reasons. Firstly, a preferential faceting is inconsistent with the catalytic properties for a reaction such as methanol synthesis. If Cu/SiO$_2$ was dominated by (311) facets and Cu/Al$_2$O$_3$ was dominated by (100) facets, then single crystal studies [91] suggest that the (311) facets, and thereby Cu/SiO$_2$, should be considerably more active. In fact it is oppositely Cu/Al$_2$O$_3$ that is an order of magnitude more active than Cu/SiO$_2$ at industrially relevant conditions [13,92]. The interpretation

in terms of preferential faceting based on $\nu_{C\text{-}O}$ thus yields an incorrect prediction of the catalytic properties.

Secondly, this interpretation neglects the importance of dipole coupling. The measurements on Raney Cu (Fig. 2) show a spectrum that appears to be dominated by the Cu(110) facet [16,46] although Wulff-construction modeling [47–49] suggests this to be the minor facet (5-8%) in comparison to Cu(100) with 25-30%, and Cu(111) with 60-70%. Because the interference phenomena from dipole coupling favor the higher frequencies it only takes a small percentage of higher frequency sites, such as the (110) facets, to dominate the spectrum. Even if the surface of a polycrystalline particle is dominated by lower frequency (100) or (111) facets it is still the minority of higher frequency (110) sites that tend to dominate the IR spectrum. For supported nanoparticles it is therefore always most likely that the major band arises from higher frequency sites, such as edges, corners, steps and the (110) facet with its rows of protrusions (or possibly Cu-O linkages to the support if present), regardless of the support. Similar coupling-favored sites are therefore likely to dominate the spectrum on all the supports, and the frequency shifts in adsorbed CO compared to the Raney Cu reference should thus reflect the support dependent modifications of these sites.

Given the relationship between charge on the surface sites and the C-O frequency (Fig. 1) it would seem likely that the variations in Table 3 reflect a gradual shift in the charging of the metal surface, from more positively charged in Cu/SiO$_2$ to more negatively charged in Cu/TiO$_2$ and Cu/ZnO(/Al$_2$O$_3$). The charge transfer from the n-type semiconductors to the metal, which could cause this charging is discussed in section 3.4. An insulator like Al$_2$O$_3$ may still have for example oxygen vacancies in the surface that can act as electron donor centers for charge transfer to supported metals as seen [93] for Au on MgO. Oppositely, the difference between Cu/SiO$_2$ (2100 cm^{-1}) and Raney Cu (2094 cm^{-1}) will mostly reflect a positive charging of the metallic Cu surface in Cu/SiO$_2$ as discussed in section 3.5.
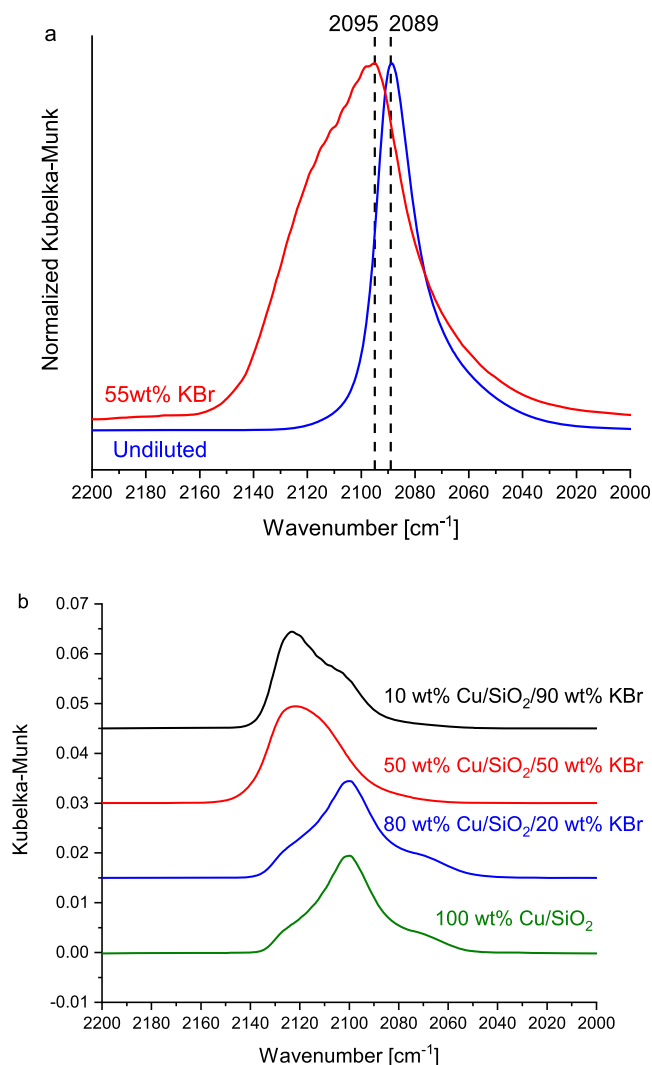
The observed differences in the abilities of the Cu surface of Cu/ZnO and Cu/SiO$_2$ towards formate uptake (Figs. 10 and 11) would also be consistent with changes in surface charging that impacts the ability to donate charge to adsorbates. It is likely that this support-dependent surface charging plays a role in regulating the interaction with the adsorbate population, which in turn may be of importance for the catalytic properties of the supported metal particles.

3.9. Effect of KBr dilution

The measurements presented in this study have been without KBr dilution. In the past literature dealing with similar IR measurements on CO adsorbed as a probe molecule it has been a common practice to use samples either physically mixed or pelletized together with KBr. However, there have been observations [32] of chemical modifications caused KBr, and it is therefore important to evaluate, if any such effects are present for CO probe molecule studies on in situ reduced samples.

Fig. 12a shows normalized IR spectra of CO adsorbed on pre-reduced, undiluted Cu/Al$_2$O$_3$ and on a physical mixture of KBr and Cu/Al$_2$O$_3$ that has been given the same pre-treatment. The figure illustrates that there are two major effects of KBr. Firstly, the KBr-diluted experiment shows a broad shoulder IR band centered around 2120 cm^{-1} indicative of CO adsorption on fully developed Cu$^+$ sites. This band is absent for the undiluted experiment. Secondly, the main IR band attributed to CO on the metallic Cu surface (see Section 3.3) is slightly shifted from 2089 cm^{-1} in the undiluted experiment to 2095 cm^{-1} in the diluted experiment. Such frequency shifts in the main frequency for CO on metallic Cu are relatively general for KBr dilution of the presently employed samples as illustrated in Table 4.

The same effects are seen in Fig. 12b, which shows IR spectra of CO adsorption on pre-reduced Cu/SiO$_2$ with varying degrees of KBr dilution. This figure clearly illustrates that the amount of fully developed Cu$^+$ sites increases with increasing amount of KBr.

a

2095 2089

55wt% KBr

Undiluted

Normalized Kubelka-Munk

Wavenumber [cm^{-1}]

b

Kubelka-Munk

10 wt% Cu/SiO$_2$/90 wt% KBr

50 wt% Cu/SiO$_2$/50 wt% KBr

80 wt% Cu/SiO$_2$/20 wt% KBr

100 wt% Cu/SiO$_2$

Wavenumber [cm^{-1}]

Fig. 12. a) IR spectra of Cu/Al$_2$O$_3$ samples diluted and undiluted in KBr and b) IR spectra of Cu/SiO$_2$ samples (normalized to the same maximum Kubelka-Munk level) during 0.4 mbar CO adsorption at 276 K but with different KBr dilution levels.

Table 4
Frequencies attributed to CO on the metallic surface of supported Cu samples with and without KBr dilution.

Sample	KBr dilution [wt%]	Metallic C-O frequency [cm^{-1}]
Cu/SiO$_2$	50	2109
Cu/SiO$_2$	0	2100
Raney Cu	50	2105
Raney Cu	0	2094
Cu/Al$_2$O$_3$	45	2095
Cu/Al$_2$O$_3$	0	2089
Cu/TiO$_2$	10	2075
Cu/TiO$_2$	0	2070
Cu/ZnO	10	2068 ± 3
Cu/ZnO	0	2065 ± 3

Transfer of potassium species to the Cu-sample is ruled out as the explanation, because this should cause a downshift in the C-O frequency [73,94], opposite to the actual observations. Instead the effects are proposed to arise from transfer of bromine to the Cu-sample, as shifts to higher C-O frequency have previously been observed [85], when co-adsorbing a halogen (Cl from methyl chloride) with CO on Cu. The transfer of presumably low levels of Br to the sample could for

example occur from hydrolysis of KBr with the water formed in the pre-reduction as illustrated by reactions R1 and R2:

$$KBr + H_2O \rightarrow KOH + HBr \qquad (R1)$$

$$HBr + Cu \rightarrow \frac{1}{2}H_2 + Br^- - Cu^+ \qquad (R2)$$

The electronic effect from an electronegative adsorbate such as a halogen will be strongest immediately at the metal atom where it is adsorbed [95], and the fully developed Cu$^+$ sites emerging in measurements on KBr diluted samples are most likely these Br$^-$-Cu$^+$ sites. However, the shift towards higher frequency for the main IR band assigned to the metallic surface could indicate that the entire Cu surface becomes more electron deficient due to the presence of the strongly electronegative adsorbates. This observation of both stronger local effects and weaker wider ranging effects could be of significance for catalytic properties of metal catalysts, which are often strongly affected by electronegative adsorbates (sulfur, halogens etc.) [96–100].

The shift in the main C-O frequency on the metallic surface is of a moderate size, and on this basis many qualitative conclusions in the literature based on KBr-diluted samples may still be valid although absolute values will be incorrect. However, the present results illustrate that the effects of dilution can be important – as an example Fig. 12b shows that KBr dilution can lead to very misleading conclusions about the distribution between metallic and oxidized sites in a sample. It is therefore advisable to regard previous studies employing KBr dilution with some caution.

4. Conclusion

Support effects on the Cu surface properties were investigated for Raney Cu and materials with Cu dispersed as nanoparticles on oxide supports using infrared spectroscopy on chemisorbed CO. Since the C-O frequency (ν_{C-O}) is sensitive to the charge on the adsorption site (ν_{C-O} higher on Cu$^+$, intermediate on Cu^0 and lower on Cu$^-$) this method can provide information about the charging state of the Cu surface. Raney Cu was used as a reference for the intrinsic properties of Cu and illustrates the challenges caused by dipole coupling. The spectrum of CO on Raney Cu is fully dominated by the contribution from CO on the (110) facets despite this being expectedly the least abundant facet on the surface. As the dipole coupling favors the higher frequency sites such as the (110) facet, the most intense spectral features arise from the most coupling-favored sites and not from the most abundant types of sites.

The most intense CO band that was present in the reduced sample, but absent in the oxidized state of the sample was taken as the main contribution from the metallic Cu surface. The frequency for this main contribution from the metallic site varies in the following order for the investigated samples: Cu/SiO$_2$ > Raney Cu > Cu/Al$_2$O$_3$ > Cu/TiO$_2$. Given the charge-frequency relation this implies that the Cu surface of Cu/SiO$_2$ is more electron depleted, whereas the Cu surface is electron enriched for Cu/TiO$_2$. These charging effects were attributed to support dependent tendencies to donate or withdraw electrons from the Cu surface. Adsorbed CO on Cu$^{\delta+}$ sites linked to basic oxides, such as ZnO, may have low frequencies, which makes spectral interpretation even more difficult. For Cu/ZnO(/Al$_2$O$_3$) systems that are important as industrial catalysts it is thus difficult to obtain an unambiguous assignment of the CO bands. However, the band that we tentatively assign to the interior of the Cu surface is lower in frequency (2065-2068 cm^{-1}) than observed on Cu single crystals, which may also indicate an electron enrichment of the Cu surface.

Experiments with co-adsorption of HCOO and CO suggested that electron-withdrawing adsorbates can accommodate the surface charge in the metal-adsorbate bonding. This conclusion is based on an increased ν_{C-O} in CO co-adsorbed with formate, which indicates that CO experiences a more electron-depleted surface because formate attracts the surface charge. A CO$_2$/H$_2$ treatment to adsorb formate on Cu/ZnO

largely prevented subsequent CO adsorption on copper sites, whereas identically treated Cu/SiO$_2$ maintained a significant fraction of its intrinsic CO adsorption. This indicates that the Cu surface of Cu/ZnO interacts more strongly with formate adsorbates, which here resulted in a greater filling of the Cu surface. This would be in reasonable agreement with a support-induced electron enrichment of the Cu surface that impacts the ability to donate charge to adsorbates. Consequently, the support dependent electron donation or withdrawal may help to regulate the interaction with adsorbates on the Cu surface and hence the catalytic properties.

The effect of sample dilution by KBr, which has been employed in many studies in the literature, was also investigated. It is observed that KBr has a substantial impact on the spectra of the in situ reduced samples. The presence of KBr leads to a growth in the number of fully developed Cu$^+$ sites and a general electron depletion of the surface (deduced from an increased ν_{C-O} for the most intense CO band). These effects were attributed to Br$^-$ transferred to the Cu surface yielding Br$^-$-Cu$^+$ at the immediate adsorption site and a wider ranging electron depleting effect.

CRediT authorship contribution statement

Niels D. Nielsen: Conceptualization, Methodology, Software, Formal analysis, Investigation, Writing - original draft, Writing - review & editing, Visualization. **Thomas E.L. Smitshuysen:** Investigation, Formal analysis. **Christian D. Damsgaard:** Supervision. **Anker D. Jensen:** Supervision, Funding acquisition, Writing - review & editing, Project administration. **Jakob M. Christensen:** Conceptualization, Supervision, Funding acquisition, Project administration, Data curation, Methodology, Visualization, Writing - review & editing.

Declaration of Competing Interest

The authors declare that they have no known competing financial interests or personal relationships that could have appeared to influence the work reported in this paper.

The authors declare the following financial interests/personal relationships which may be considered as potential competing interests.

Acknowledgements

Supplementary materials

Supplementary material associated with this article can be found, in the online version, at doi:10.1016/j.susc.2020.121725.

References

[1] B.S. Clausen, G. Steffensen, B. Fabius, J. Villadsen, R. Feidenhans'l, H. Topsøe, In situ cell for combined XRD and on-line catalysis tests: Studies of Cu-based water gas shift and methanol catalysts, J. Catal. 132 (1991) 524–535 https://doi.org/10.1016/0021-9517(91)90168-4.

[2] V. Kleymenov, J. Sa, J. Abu-Dahrieh, D. Rooney, J.A. Van Bokhoven, E. Troussard, J. Szlachetko, O.V. Safonova, M. Nachtegaal, Structure of the methanol synthesis catalyst determined by in situ HERFD XAS and EXAFS, Catal. Sci. Technol. 2 (2012) 373–378 https://doi.org/10.1039/c1cy00277e.

[3] J.L. Robbins, E. Iglesia, C.P. Kelkar, B. DeRites, Methanol synthesis over Cu/SiO$_2$ catalysts, Catal. Letters 10 (1991) 1–10 https://doi.org/10.1007/BF00764730.

[4] C. Baltes, S. Vukojević, F. Schüth, Correlations between synthesis, precursor, and catalyst structure and activity of a large set of CuO/ZnO/Al$_2$O$_3$ catalysts for methanol synthesis, J. Catal. 258 (2008) 334–344 https://doi.org/10.1016/j.jcat.2008.07.004.

[5] R.W. Joyner, R. Burch, S.E. Golunski, M.S. Spencer, "Good" correlations in methanol synthesis catalysis, a comment on a letter by burch, golunski and spencer, Catal. Lett. 6 (1990) 151–156 https://doi.org/10.1007/BF00764064.

[6] M.J.L. Ginés, N. Amadeo, M. Laborde, C.R. Apesteguía, Activity and structure-sensitivity of the water-gas shift reaction over Cu–Zn–Al mixed oxide catalysts,

[7] F.S. Stone, D. Waller, Cu-ZnO and Cu-ZnO/Al$_2$O$_3$ catalysts for the reverse water-gas shift reaction. The effect of the Cu/Zn ratio on precursor characteristics and on the activity of the derived catalysts, Top. Catal. 22 (2003) 305–318 https://doi.org/10.1023/A:1023592407825.

[8] R.A. Hadden, P.J. Lambert, C. Ranson, Relationship between the copper surface area and the activity of CuO/ZnO/Al$_2$O$_3$ water-gas shift catalysts, Appl. Catal. A, Gen. 122 (1995) L1–L4 https://doi.org/10.1016/0926-860X(94)00263-0.

[9] T. Fujitani, M. Saito, Y. Kanai, T. Kakumoto, T. Watanabe, J. Nakamura, T. Uchijima, The role of metal oxides in promoting a copper catalyst for methanol synthesis, Catal. Lett. 25 (1994) 271–276 https://doi.org/10.1007/BF00816307.

[10] P. Chaumette, J. Barbier, J. Fortin, Carbonates, a key for selecting methanol synthesis catalysts, in: M. Phillips, J.M. Ternan (Eds.), Proc 9th Int Congr Catal. 2 The Chemical Institute of Canada, 1988, pp. 585–593.

[11] K.M.M. Saito, Development of high performance Cu/ZnO-based catalysts for methanol synthesis and the water-gas shift reaction, Catal. Surv. Asia 8 (4) (2004) 285–294 https://doi.org/10.1007/s10563-004-9119-y.

[12] Roy van den Berg, G. Prieto, G. Korpershoek, L.I. Van Der Wal, A.J. Van Bunningen, S. Lægsgaard-Jørgensen, P.E. De Jongh, K.P. De Jong, Structure sensitivity of Cu and CuZn catalysts relevant to industrial methanol synthesis, Nat. Commun. 7 (2016) 1–7 https://doi.org/10.1038/ncomms13057.

[13] J. Thrane, S. Kuld, N.D. Nielsen, A.D. Jensen, J. Sehested, J.M. Christensen, Methanol assisted autocatalysis in catalytic methanol synthesis, Angew. Chemie - Int. Ed. (2020) in press https://doi.org/10.1002/anie.202006921.

[14] K. Hadjiivanov, T. Venkov, H. Knözinger, FTIR spectroscopy study of CO adsorption on Cu/SiO$_2$: Formation of new types of copper carbonyls, Catal. Lett. 75 (2001) 55–59 https://doi.org/10.1023/A:1016759123842.

[15] K.I. Hadjiivanov, M.M. Kantcheva, D.G. Klissurski, IR study of CO adsorption on Cu-ZSM-5 and CuO/SiO$_2$ catalysts: J. Chem. Soc. Faraday Trans. 92 (1996) 4595–4600 https://doi.org/10.1039/FT9969204595.

[16] P. Hollins, J. Pritchard, Infrared studies of chemisorbed layers on single crystals, Prog. Surf. Sci. 19 (1985) 275–350 https://doi.org/10.1016/0079-6816(85)90015-2.

[17] M. Head-Gordon, J.C. Tully, Electric field effects on chemisorption and vibrational relaxation of CO on Cu(100), Chem. Phys. 175 (1993) 37–51 https://doi.org/10.1016/0301-0104(93)80227-Z.

[18] J. Dong, L. Miao, M. Zhou, Infrared spectra and density functional calculations of the Cu(CO)$_{1-4}^+$,Cu(CO)$_{1-3}$, and Cu(CO)$_{1-3}^-$ in solid neon, Chem. Phys. Lett. 355 (2002) 31–36 https://doi.org/10.1016/S0009-2614(02)00145-8.

[19] G. Busca, FT-IR study of the surface of copper oxide, J. Mol. Catal. 43 (1987) 225–236 https://doi.org/10.1016/0304-5102(87)87010-4.

[20] A.A. Davydov, Study of the state of transitions-metal cations on catalys surfaces by the IR spectroscopy of adsorbed test molecules (CO, NO). VI. State of copper in CuO. Influence of Supports on the state of copper, Kinet. Catal. 26 (1985) 157–167 (135–144 in Engl. transl.).

[21] R. Smoluchowski, Anisotropy of the electronic work function of metals, Phys. Rev. 60 (1941) 661–674 https://doi.org/10.1103/PhysRev.60.661.

[22] C.J. Fall, N. Binggeli, A. Baldereschi, Work Functions at Facet Edges, Phys. Rev. Lett. 88 (2002) 156802https://doi.org/10.1103/PhysRevLett.88.156802.

[23] L. Gao, J. Souto-Casares, J.R. Chelikowsky, A.A. Demkov, Orientation dependence of the work function for metal nanocrystals, J. Chem. Phys. 147 (2017) 214301https://doi.org/10.1063/1.4991725.

[24] G. Blyholder, Molecular Orbital View of Chemisorbed Carbon Monoxide, J. Phys. Chem. 68 (1964) 2772–2777 https://doi.org/10.1021/j100792a006.

[25] R. Van Santen, N. Matthew, Molecular Heterogeneous Catalysis: A Conceptual and Computational Approach, Wiley-VCH, 2006, https://doi.org/10.1002/9783527610846.

[26] V.M. Browne, S.G. Fox, P. Hollins, Coupling effects in infrared spectra from supported metal catalysts, Mater. Chem. Phys. 29 (1991) 235–244 https://doi.org/10.1016/0254-0584(91)90019-Q.

[27] P. Hollins, Effects of dipolar coupling on the intensity of infrared absorption bands from supported metal catalysts, Spectrochim. Acta - Part A Mol. Spectrosc. 43 (1987) 1539–1542 https://doi.org/10.1016/S0584-8539(87)80044-2.

[28] X. Xu, S. Vesecky, D. Goodman, Infrared Reflection-Absorption Spectroscopy and STM Studies of Model Silica-Supported Copper Catalysts, Science 258 (1992) 788–790 https://doi.org/10.1126/science.258.5083.788.

[29] D.F. Cox, K.H. Schulz, Interaction of CO with Cu$^+$ cations: CO adsorption on Cu$_2$O (100), Surf. Sci. 249 (1991) 138–148 https://doi.org/10.1016/0039-6028(91)90839-K.

[30] N.-Y. Topsøe, H. Topsøe, FTIR studies of dynamic surface structural changes in Cu-based methanol synthesis catalysts, J. Mol. Catal. A Chem. 141 (1999) 95–105 https://doi.org/10.1016/s1381-1169(98)00253-2.

[31] J. Schumann, J. Kröhnert, E. Frei, R. Schlögl, A. Trunschke, IR-Spectroscopic Study on the Interface of Cu-Based Methanol Synthesis Catalysts: Evidence for the Formation of a ZnO Overlayer, Top. Catal. 60 (2017) 1735–1743 https://doi.org/10.1007/s11244-017-0850-9.

[32] J. Couble, P. Gravejat, F. Gaillard, D. Bianchi, Quantitative analysis of infrared spectra of adsorbed species using transmission and diffuse reflectance modes case study: Heats of adsorption of CO on TiO$_2$ and CuO/Al$_2$O$_3$, Appl. Catal. A Gen. 371 (2009) 99–107 https://doi.org/10.1016/j.apcata.2009.09.036.

[33] F.C. Meunier, Pitfalls and benefits of in situ and operando diffuse reflectance FT-IR spectroscopy (DRIFTS) applied to catalytic reactions, React. Chem. Eng. 1 (2016) 134–141 https://doi.org/10.1039/C5RE00018A.

[34] N.D. Nielsen, A.D. Jensen, J.M. Christensen, Quantification of Formate and Oxygen Coverages on Cu Under Industrial Methanol Synthesis Conditions, Catal. Lett. 150

(2020) 2447–2456 https://doi.org/10.1007/s10562-020-03162-7.

[35] G.C. Chinchen, C.M. Hay, H.D. Vandervell, K.C. Waugh, The measurement of copper surface areas by reactive frontal chromatography, J. Catal. 103 (1987) 79–86 https://doi.org/10.1016/0021-9517(87)90094-7.

[36] R. Chatterjee, S. Kuld, R. Van Den Berg, A. Chen, W. Shen, Mapping Support Interactions in Copper Catalysts, Top. Catal. 62 (2019) 649–659 https://doi.org/10.1007/s11244-019-01150-9.

[37] O. Hinrichsen, T. Genger, M. Muhler, Chemisorption of N₂O and H₂ for the Surface Determination of Copper Catalysts, Chem. Eng. Technol. 23 (2000) 956–959 https://doi.org/10.1002/1521-4125(200011)23:11<956::AID-CEAT956>3.0.CO;2-L.

[38] P. Scherrer, Bestimmung der Grösse und der inneren Struktur von Kolloidteilchen mittels Röntgenstrahlen, Nachr. Ges. Wiss. Gött. 26 (1918) 98–100.

[39] B.D. Cullity, Element of X-ray Diffraction, 2nd Edition, Addison-Wesley, 1978.

[40] H.P. Klug, L.E. Alexander, X-Ray Diffraction Procedures: For Polycrystalline and Amorphous Materials, 2nd Edition, Wiley, 1974.

[41] A. Belkly, M. Helderman, V.L. Karen, P. Ulkch, New developments in the Inorganic Crystal Structure Database (ICSD): Accessibility in support of materials research and design, Acta Crystallogr. Sect. B Struct. Sci. 58 (2002) 364–369 https://doi.org/10.1107/S0108768102006948.

[42] Q. Wu, L.D.L. Duchstein, G.L. Chiarello, J.M. Christensen, C.D. Damsgaard, C.F. Elkjær, J.B. Wagner, B. Temel, J.D. Grunwaldt, A.D. Jensen, In situ observation of Cu-Ni alloy nanoparticle formation by X-ray diffraction, X-ray absorption spectroscopy, and transmission electron microscopy: Influence of Cu/Ni ratio, ChemCatChem. 6 (2014) 301–310 https://doi.org/10.1002/cctc.201300628.

[43] A. Karelovic, P. Ruiz, The role of copper particle size in low pressure methanol synthesis via CO₂ hydrogenation over Cu/ZnO catalysts, Catal. Sci. Technol. 5 (2015) 869–881 https://doi.org/10.1039/C4CY00848K.

[44] A. Karelovic, G. Galdames, J.C. Medina, C. Yévenes, Y. Barra, R. Jiménez, Mechanism and structure sensitivity of methanol synthesis from CO₂ over SiO₂-supported Cu nanoparticles, J. Catal. 369 (2019) 415–426 https://doi.org/10.1016/j.jcat.2018.11.012.

[45] X. Xu, D.W. Goodman, Structural and chemisorptive properties of model catalysts: Copper supported on SiO₂ thin films, J. Phys. Chem. 97 (1993) 683–689 https://doi.org/10.1021/j100105a025.

[46] J. Pritchard, T. Catterick, R.K. Gupta, Infrared Spectroscopy of Chemisorbed CO on Cu, Surf. Sci. 53 (1975) 1–20 https://doi.org/10.1108/17561370910989284.

[47] J.J.F. Scholten, J.A. Konvalinka, Reaction of nitrous oxide with a nickel surface, Trans. Faraday Soc. 65 (1969) 2465–2473 https://doi.org/10.1016/S0166-9834(00)82418-5.

[48] B.E. Sundquist, A direct determination of the anisotropy of the surface free energy of solid gold, silver, copper, nickel, and alpha and gamma iron, Acta Metall. 12 (1964) 67–86 https://doi.org/10.1016/0001-6160(64)90055-0.

[49] C.V. Ovesen, B.S. Clausen, J. Schiøtz, P. Stoltze, H. Topsøe, J.K. Nørskov, Kinetic Implications of Dynamical Changes in Catalyst Morphology during Methanol Synthesis over Cu/ZnO Catalysts, J. Catal. 168 (1997) 133–142 https://doi.org/10.1006/jcat.1997.1629.

[50] R.N. D'Alnoncourt, X. Xia, J. Strunk, E. Löffler, O. Hinrichsen, M. Muhler, The influence of strongly reducing conditions on strong metal-support interactions in Cu/ZnO catalysts used for methanol synthesis, Phys. Chem. Chem. Phys. 8 (2006) 1525–1538 https://doi.org/10.1039/b515487a.

[51] M.B. Padley, C.H. Rochester, G.J. Hutchings, F. King, FTIR Spectroscopic Study of Thiophene, SO₂, and CO Adsorption on Cu/Al₂O₃ Catalysts, J. Catal. 148 (1994) 438–452 https://doi.org/10.1006/jcat.1994.1230.

[52] O. Dulaurent, X. Courtois, V. Perrichon, D. Bianchi, Heats of adsorption of CO on a Cu/Al₂O₃ catalyst using FTIR spectroscopy at high temperatures and under adsorption equilibrium conditions, J. Phys. Chem. B. 104 (2000) 6001–6011 https://doi.org/10.1021/jp9943629.

[53] H. Arakawa, K. Sayama, K. Okabe, A. Murakami, Promoting effect of TiO₂ addition to CuO-ZnO catalyst on methanol synthesis by catalytic hydrogenation of CO₂, Stud. Surf. Sci. Catal. 77 (1993) 389–392 https://doi.org/10.1016/S0167-2991(08)63218-8.

[54] K. Hadjiivanov, J. Lamotte, J.C. Lavalley, FTIR study of low-temperature CO adsorption on pure and ammonia-precovered TiO₂ (anatase), Langmuir 13 (1997) 3374–3381 https://doi.org/10.1021/la962104m.

[55] J.C. Frost, Junction effect interactions in methanol synthesis catalysts, Nature 334 (1988) 577–580 https://doi.org/10.1038/332141a0.

[56] M.W. Allen, S.M. Durbin, Influence of oxygen vacancies on Schottky contacts to ZnO, Appl. Phys. Lett. 92 (2008) 1–4 https://doi.org/10.1063/1.2894568.

[57] F. Boccuzzi, G. Ghiotti, A. Chiorino, Metal-semiconductor interaction: Effect of H₂ chemisorption on the IR transparency of the Cu/ZnO system, Surf. Sci. Lett. 183 (1987) 285–289 https://doi.org/10.1016/0167-2584(87)90133-2.

[58] T. Binninger, T.J. Schmidt, D. Kramer, Capacitive electronic metal-support interactions: Outer surface charging of supported catalyst particles, Phys. Rev. B 96 (2017) 165405 https://doi.org/10.1103/PhysRevB.96.165405.

[59] G. Ghiotti, F. Boccuzzi, A. Chiorino, The Operation of the "Metal-Surface Selection Rule" on the Vibrational Spectra of Species Adsorbed on Supported Copper Particles, Surf. Sci. 178 (1986) 553–564 https://doi.org/10.1016/0039-6028(86)90332-8.

[60] J. Saussey, J.C. Lavalley, J. Lamotte, T. Rais, I.R. Spectroscopic Evidence of Formyl Species formed by CO and H₂, Co-adsorption on ZnO and Cu-ZnO, J. Chem. Soc. Chem. Commun. 5 (1982) 278–279 https://doi.org/10.1039/C39820000278.

[61] F. Boccuzzi, E. Garrone, A. Zecchina, A. Bossi, M. Camia, Infrared study of ZnO surface properties. II. H₂-CO interaction at room temperature, J. Catal. 51 (1978) 160–168 https://doi.org/10.1016/0021-9517(78)90289-0.

[62] F. Boccuzzi, G. Ghiotti, A. Chiorino, CO adsorption on small particles of Cu dispersed on microcrystalline ZnO, Surf. Sci. 156 (1985) 933–942 https://doi.org/10.1016/0039-6028(85)90269-9.

[63] N.D. Nielsen, J. Thrane, A.D. Jensen, J.M. Christensen, Bifunctional Synergy in CO Hydrogenation to Methanol with Supported Cu, Catal. Lett. 150 (2020) 1427–1433 https://doi.org/10.1007/s10562-019-03036-7.

[64] A.M. Abdel-Mageed, A. Klyushin, A. Rezvani, A. Knop-Gericke, R. Schlögl, R.J. Behm, Negative Charging of Au Nanoparticles during Methanol Synthesis from CO₂/H₂ on a Au/ZnO Catalyst: Insights from Operando IR and Near-Ambient-Pressure XPS and XAS Measurements, Angew. Chemie - Int. Ed. 58 (2019) 10325–10329 https://doi.org/10.1002/anie.201900150.

[65] B.E. Goodby, J.E. Pemberton, XPS Characterization of a Commercial Cu/ZnO/Al₂O₃ Catalyst: Effects of Oxidation, Reduction, and the Steam Reformation of Methanol, Appl. Spectrosc. 42 (1988) 754–760 https://doi.org/10.1366/0003702884429148.

[66] Y. Okamoto, K. Fukino, T. Imanaka, S. Teranishi, Surface Characterization of CuO-ZnO Methanol-Synthesis Catalysts by X-ray Photoelectron Spectrosocpy. 2. Reduced Catalysts, J. Phys. Chem. 87 (1983) 3747–3754 https://doi.org/10.1021/j100242a035.

[67] L.H. Dubois, B.R. Zegarski, R.G. Nuzzo, Spontaneous Organization of Carboxylic Acid Monolayer Films in Ultrahigh Vacuum. Kinetic Constraints to Assembly via Gas-Phase Adsorption, Langmuir 2 (1986) 412–417 https://doi.org/10.1021/la00070a006.

[68] M. Bowker, H. Houghton, K.C. Waugh, Mechanism and kinetics of methanol synthesis on zinc oxide, J. Chem. Soc. Faraday Trans. 1 Phys. Chem. Condens. Phases 77 (1981) 3023–3036 https://doi.org/10.1039/F19817703023.

[69] K. Kähler, M.C. Holz, M. Rohe, J. Strunk, M. Muhler, Probing the reactivity of ZnO and Au/ZnO nanoparticles by methanol adsorption: A TPD and DRIFTS study, ChemPhysChem. 11 (2010) 2521–2529 https://doi.org/10.1002/cphc.201000282.

[70] S. Fujita, M. Usui, H. Ito, N. Takezawa, Mechanisms of Methanol Synthesis from Carbon Dioxide and from Carbon Monoxide at Atmospheric Pressure over Cu/ZnO, J. Catal. 157 (1995) 403–413 http://dx.doi.org/10.1006/jcat.1995.1306.

[71] K.K. Bando, K. Sayama, H. Kusama, K. Okabe, H. Arakawa, In-situ FT-IR study on CO₂ hydrogenation over Cu catalysts supported on SiO₂, Al₂O₃, and TiO₂, Appl. Catal. 165 (1997) 391–409 https://doi.org/10.1016/S0926-860X(97)00221-4.

[72] S. Fujita, M. Usui, E. Ohara, N. Takezawa, Methanol synthesis from carbon dioxide at atmospheric pressure over Cu/ZnO catalyst. Role of methoxide species formed on ZnO support, Catal. Lett. 13 (1992) 349–358 https://doi.org/10.1007/BF00765037.

[73] D.B. Clarke, A.T. Bell, An Infrared Study of Methanol Synthesis from CO₂ on Clean and Potassium-Promoted Cu/SiO₂, J. Catal. 154 (1995) 314–328 https://doi.org/10.1006/jcat.1995.1173.

[74] F. Boccuzzi, A. Chiorino, S. Tsubota, M. Haruta, FTIR Study of Carbon Monoxide Oxidation and Scrambling at Room Temperature over Gold Supported on ZnO and TiO₂, J. Phys. Chem. 100 (2002) 3625–3631 https://doi.org/10.1021/jp952259n.

[75] M. Shim, P. Guyot-Sionnest, Organic-capped ZnO nanocrystals: Synthesis and n-type character, J. Am. Chem. Soc. 123 (2001) 11651–11654 https://doi.org/10.1021/ja0163321.

[76] D.A. Panayotov, S.P. Burrows, J.R. Morris, Infrared spectroscopic studies of conduction band and trapped electrons in UV-photoexcited, H-Atom n-doped, and thermally reduced TiO₂, J. Phys. Chem. C. 116 (2012) 4535–4544 https://doi.org/10.1021/jp2053103.

[77] F. Boccuzzi, C. Morterra, R. Scala, A. Zecchina, Infrared Spectrum of Microcrystalline Zinc Oxide, Chem. Soc. Faraday Trans. 77 (1981) 2059–2066 2.

[78] B.A. Morrow, Infra-red studies of reactions on oxide surfaces. Part 2.-Methanol on silica, J. Chem. Soc. Faraday Trans. 1 Phys. Chem. Condens. Phases 70 (1974) 1527–1545 https://doi.org/10.1039/F19747001527.

[79] I.A. Fisher, A.T. Bell, In Situ Infrared Study of Methanol Synthesis from H₂/CO over Cu/SiO₂ and Cu/ZrO₂/SiO₂, J. Catal. 178 (1998) 153–173 https://doi.org/10.1006/jcat.1998.2134.

[80] L.D. White, C.P. Tripp, A low-frequency infrared study of the reaction of methoxymethylsilanes with silica, J. Colloid Interface Sci. 224 (2000) 417–424 https://doi.org/10.1006/jcis.1999.6709.

[81] L.H. Dubois, T.H. Ellis, B.R. Zegarski, S.D. Kevan, New insights into the kinetics of formic acid decomposition on copper surfaces, Surf. Sci. 172 (1986) 385–397 https://doi.org/10.1016/0039-6028(86)90763-6.

[82] E.T. Krastev, D.E. Kuhl, R.G. Tobin, Multiple mechanisms for adsorbate-induced resistivity: Oxygen and formate on Cu(100), Surf. Sci. 387 (1997) L1051–L1056 https://doi.org/10.1016/S0039-6028(97)00439-1.

[83] A. Chutia, I.P. Silverwood, M.R. Farrow, D.O. Scanlon, P.P. Wells, M. Bowker, S.F. Parker, C.R.A. Catlow, Adsorption of formate species on Cu(h,k,l) low index surfaces, Surf. Sci. 653 (2016) 45–54 https://doi.org/10.1016/j.susc.2016.05.002.

[84] M. Bowker, R.J. Madix, XPS, UPS and thermal desorption studies of the reactions of formaldehyde and formic acid with the Cu(110) surface, Surf. Sci. 102 (1981) 542–565 https://doi.org/10.1016/0039-6028(81)90045-5.

[85] L. Dubois, B.R. Zegarski, The influence of electron-withdrawing on the adsorption of CO on copper, Chem. Phys. Lett. 120 (1985) 537–541 https://doi.org/10.1016/0009-2614(85)80550-9.

[86] Y. Amenomiya, Infrared study of methanol synthesis from CO₂ and H₂ on supported copper-zinc oxide catalysts, in: G. Ertl (Ed.), Proc. 8th Int. Congr. Catal. 2 Verlag Chemie, 1984, pp. 557–567.

[87] J. Nakamura, J.M. Campbell, C.T. Campbell, Kinetics and mechanism of the water-gas shift reaction catalysed by the clean and Cs-promoted Cu(110) surface: A comparison with Cu(111), J. Chem. Soc. Faraday Trans. 86 (1990) 2725–2734 https://doi.org/10.1039/FT9908602725.

[88] S.I. Fujita, M. Usui, N. Takezawa, Mechanism of the reverse water gas shift reaction over Cu/ZnO catalyst, J. Catal. 134 (1992) 220–225 https://doi.org/10.1016/0021-9517(92)90223-5.

[89] C.V. Ovesen, P. Stoltze, J.K. Nørskov, C.T. Campbell, A kinetic model of the water gas shift reaction, J. Catal. 134 (1992) 445–468 https://doi.org/10.1016/0021-9517(92)90334-E.

[90] C. Truong, J. Rodriguez, D. Goodman, CO adsorption isotherms on Cu(100) at elevated pressures and temperatures using infrared reflection absorption spectroscopy, Surf. Sci. Lett. 271 (1992) L385–L391 https://doi.org/10.1016/0039-6028(92)90896-E.

[91] I. Nakamura, T. Fujitani, T. Uchijima, J. Nakamura, A model catalyst for methanol synthesis: Zn-deposited and Zn-free Cu surfaces, J. Vac. Sci. Technol. 14 (1996) 1464–1468 https://doi.org/10.1116/1.579970.

[92] M. Saito, J. Wu, K. Tomoda, I. Takahara, K. Murata, Effects of ZnO contained in supported Cu-based catalysts on their activities for several reactions, Catal. Lett. 83 (2002) 1–4 https://doi.org/10.1023/A:1020693226903.

[93] B. Yoon, H. Häkkinen, U. Landman, A.S. Wörz, J.M. Antonietti, S. Abbet, K. Judai, U. Heiz, Charging effects on bonding and catalyzed oxidation of CO on Au$_8$ clusters on MgO, Science 307 (2005) 403–407 https://doi.org/10.1126/science.1104168.

[94] L.H. Dubois, B.R. Zegarski, H.S. Luftman, Summary Abstract: Multiple CO bonding states on potassium-dosed Cu(100), J. Vac. Sci. Technol. A 5 (1987) 455–457 https://doi.org/10.1116/1.574688.

[95] J.K. Nørskov, S. Holloway, Microscopic Model for the Poisoning and Promotion of Adsorption Rates by Electronegative and Electropositive Atoms, Surf. Sci. 137 (1984) 65–78 https://doi.org/10.1016/0039-6028(84)90676-9.

[96] J.C.J. Bart, R.P.A. Sneeden, Copper-zinc oxide-alumina methanol catalysts revisited, Catal. Today. 2 (1987) 1–124 https://doi.org/10.1016/0920-5861(87)80001-9.

[97] J.B. Hansen, P. Nielsen E. H., H. Nielsen, Methanol Synthesis, G. Ertl, H. Knözinger, J. Weitkamp (Eds.), 2nd ed., Wiley-VCH Verlag GmbH, 2008, pp. 2920–2949 https://doi.org/10.1002/9783527610044.hetcat0148.

[98] D.E. Peebles, D.W. Goodman, J.M. White, Methanation of carbon dioxide on Ni (100) and the effects of surface modifiers, J. Phys. Chem. 87 (1983) 4378–4387 https://doi.org/10.1021/j100245a014.

[99] D.W. Goodman, M. Kiskinova, Chemisorption and reactivity studies of H$_2$ and CO on sulfided Ni(100), Surf. Sci. 105 (1981) L265–L270 https://doi.org/10.1016/0039-6028(81)90001-7.

[100] M. Kiskinova, D.W. Goodman, Modification of chemisorption properties by electronegative adatoms: H$_2$ and CO on chlorided, sulfided, and phosphided Ni(100), Surf. Sci. 108 (1981) 64–76 https://doi.org/10.1016/0039-6028(81)90358-7.